Smart Nanotechnologies to Target Tumor with Deep Penetration Depth for Efficient Cancer Treatment and Imaging

Smart nanotechnologies to target tumor with deep penetration depth for efficient cancer treatment and imaging

*Xue Feng, Hannah Dixon, Harriet Glen-Ravenhill, Sena Karaosmanoglu, Quan Li, Li Yan, Xianfeng Chen**

Xue Feng, Hannah Dixon, Harriet Glen-Ravenhill, Sena Karaosmanoglu, Dr. Xianfeng Chen
School of Engineering, Institute for Bioengineering, The University of Edinburgh, King's Buildings, Mayfield Road, Edinburgh EH9 3JL, United Kingdom
Email: xianfeng.chen@oxon.org or Michael.Chen@ed.ac.uk

Dr. Xianfeng Chen
Translational Medicine Center, The Second Affiliated Hospital, Guangzhou Medical University, Guangzhou, P.R. China

Dr. Quan Li
School of Engineering, Institute for Energy Systems, The University of Edinburgh, King's Buildings, Mayfield Road, Edinburgh EH9 3JL, United Kingdom

Dr. Li Yan
Monash Institute of Pharmaceutical Sciences, Monash University, Parkville, Victoria 3052, Australia

Keywords: Nanoparticles; nanomedicine; deep penetration; tumor; tumor microenvironment; cancer

Abstract:

Nanomedicines have long been expected to significantly enhance cancer treatment. However, their clinical translation is still very limited despite of the world's great efforts during the last 2 decades. One of the reasons is that the transport barriers within tumors restrict their penetration into tumors, with most nanomedicines remaining among the top submicrometer to several micrometers scale. Therefore, there is an extensive interest in the field to understand the tumor microenvironment and develop techniques to boost the penetration of nanomedicines in tumors. This review emphasizes the need of smart nanotechnology to fit the changing requirements of nanomedicines for effective drug delivery, particularly the technologies for deep penetration of nanomedicines in tumor tissues, and explores their mechanisms in order to achieve multistage requirement during the applications of nanomedicines in patients. Finally, the advantages and

disadvantages of current approaches to facilitate the deep penetration of nanomedicines are discussed and possible future avenues for smart nanotechnology are identified.

1. Introduction

Cancer is the second-leading cause of mortality in the world; 1 in 6 deaths worldwide is a result of cancer which equates to 9.6 million deaths per year.[1] Apart from surgery, chemotherapy is extremely important for patients who are unsuitable for surgery and for tumors that cannot be completely removed, while the non-targeted nature of chemotherapeutic drugs often causes systemic toxicity due to the inability to differentiate healthy cells from tumor cells. Gratefully, due to the fast development of nanotechnology, i.e. targeted delivery fulfilled by nanomedicines, the efficacy of cancer chemotherapeutics is expected to be improved. Nanoparticles (NPs) are defined as those measured in the nanoscale between 1 – 1000 nm, which have the flexibility of surface modification.[2-3] Approved anti-cancer drugs can be loaded onto or into NPs, as they are often referred to as 'nanocarriers'. Commonly, nanocarriers are fabricated into 10 to 250 nm and could largely increase their accumulation on the tumor site via various targeting mechanisms, improved drug stability, and increased blood circulation half-life.[4-6] These advantages can potentially relieve clinical side effects caused by traditional small molecule chemotherapeutic drugs including high damage to health tissues and short blood circulation half-life.[7-8]

However, the therapeutic efficacy of numerous nanomedicines in the clinical setting is still quite limited despite the fact that nanomedicines are able to more efficiently transport to tumor regions. This is most attributed to the ineffective intratumoral penetration of the nanomedicines since it is not an easy task to cross several transport barriers within tumors and then work on the tumor cell parenchyma. Tumor cells are located in the deep area of tumor tissue which is protected by a dense tumor extracellular matrix (ECM), elevated interstitial fluid pressure (IFP), hypoxic and avascular zones, and a variety of stromal cells.[9-15] These factors

restrict the transport of nanomedicines to the tumor cells through diffusion or convection and they may cause drugs to be extravasated back into the blood stream. Typically, the penetration depth of most targeted nanomedicines is only on the submicrometer to several micrometers scale (typically 3–5 cell diameters).[16] For example, Doxil® is a commercial passively targeted PEGylated liposomal nanomedicine, its penetration depth in mice tumor xenografts is limited to 18.8 μm. With prolonging time, the drug could diffuse back toward the vascular wall.[17-18] Thus, it is hard to desire that nanomedicines would kill all tumor cells and cure cancer with the current technique. Tumor is more likely to return after treatment. Consequently, the improvement of intratumoral penetration of nanomedicines, allowing them to perform their maximum anti-cancer efficiency, could be one of the most critical and tough tasks in current chemotherapeutic research.

Prior strategies for achieving deep penetration depth can be divided into four main categories. The first is to tune the physico-chemical properties of nanomedicines. There is a wave of works demonstrating that NPs with small size, non-round shape and positive surface charge are associated with better tumor penetration. However, these optimal characteristics of nanomedicines for penetration compromised their tumor delivery efficiency. The reasons are that small NPs under 5 nm could be easily cleared in blood circulation and positively charged NPs will interact with the negatively charged biological system.[19-20] In other words, one-size or one-charge NP drug transport is hardly fitting the whole in vivo journey. To tackle this, many studies about dynamic regulation of NPs' physico-chemical properties and intratumoral drug release have been reported using tumoral internal triggers (e.g., lower pH than blood, high concentration of matrix metalloproteinases, and redox) or external triggers (e.g., light, temperature, and ultrasounds).[21-22] As a result, the small or positive charged nanomedicines are only exposed to the tumor regions for improved penetration ability and have no influence to circulation and targeting efficiency. The second type of methods is to modulate the tumor microenvironment via pharmacological or physical treatment (ultrasound, radiation or

hyperthermia), such as degrading dense ECM to reduce penetration hindrances, and normalizing abnormal vasculature to lower the IFP and to increase vascular permeability. The third class of strategies is to use magnetic force to drive deep penetration of nanomedicines into humoral hypoxic and avascular zones. The magnetic drug targeting method was proposed as far back as 1978,[23] but the works that examined magnetic drug targeting to improve tumor penetration were only reported in the past decade and this field is still at infancy. The fourth type of strategies is the recently developed biological approaches.

This review systematically describes the barriers to tumor penetration and subsequently evaluates the effects of smart nanotechnologies to reach deep penetration depths within tumors in order to achieve efficient cancer treatment. Then the advantages and disadvantages of each approach is discussed, followed by our insights into the key issues of these technologies and the future development for clinical applications. The structure and contents of the review are summarized in Figure 1.

2. Challenges and requirements for deep penetration of NPs

Nanodrugs are transported to their target tumor cells in three sequential steps: vascular transport, trans-vascular transport and interstitial transport (Figure 2). The first of these involves the flow of NPs to tumor regions via blood vessels. Once this has been achieved, they must then pass through the vessel wall. Finally, the NPs must penetrate through the interstitial space between tissues in order to reach target tumor cells.[24] To ensure the final delivery of nanodrugs to deep tumor cells, different challenges and requirements for each stages in transport of NPs should be recognized and addressed.

2.1 Barriers outside the tumor

Before targeting tumor sites, NPs undergo many hurdles. First, all NPs have a half-life which governs their biodistribution and how long they circulate. The rapid clearance of NPs could take place through the mononuclear phagocyte system (MPS) and reticuloendothelial

system (RES).[25-28] The RES system, found in the liver and the spleen, is important for normal function of the body, but the main culprit of NP clearance. The surface charge plays a huge role in determining the fate of the NPs with respect to the RES system. Large zeta potentials, positive or negative, causes more RES/NP interactions and therefore more clearance.[24] Another undesirable clearance is kidney filtration, while it can be reduced by careful consideration of particle size. The effective pore size of the glomerular wall is 8 nm; therefore, particles larger than this are less likely to pass through than smaller particles.[19] Second, NPs will come into contact with normal cells, and there is a risk of toxicity if the NPs are non-targeting to tumor tissue. Thus, NPs must show stability in the conditions within the blood stream. Blood vessels have a pH of approximately 7.4 and a negatively-charged luminal surface.[29] Surface modifications must stay attached under this condition, or the NPs would disintegrate and release cytotoxic drugs to the rest of the body. For sufficient permeability, a longer blood circulation is recommended. As a result, the requirements for NPs at these stages of transport are pH stable and neutrally or negatively charged surface modifications to alleviate the attraction of blood vessels, and larger size of more than 10 nm to prevent the clearance from blood circulation.[30]

After blood circulation, the next stage is to preferentially transport to tumor sites. For this, two mechanisms have been proposed: passive targeting and active targeting. In passive (or physical) targeting, nanocarriers – a nanoscale transporter of drugs – can access tumors via the surrounding leaky vasculature (pore size on tumoral microvessels ranges from 100 to 1200 nm) due to the enhanced permeability and retention (EPR) effect (Figure 2).[31] However, the enhanced permeability of leaky tumor vasculature allows macromolecules to transport into the tumor interstitial space but is unable to facilitate permeation. Additionally, this model has now been seriously challenged as the EPR effect is not observed in clinical settings.[32] Danhier proposed that the EPR effect only works in rodents rather than humans based on thousands of research papers.[33] While another opinion is that the EPR effect may be existing for some tumors but not for others.[34]

Based on the knowledge of blood circulation and tumor targeting of anticancer drugs, various types of nanomedicines have been developed. The first-generation nanomedicines were launched about 30 years ago and some of them have been commercialized such as Doxil®/Caelyx® and Myocet® (PEGylated liposomal doxorubicin), and Abraxane® (nanoparticle albumin-binding paclitaxel).[35-38] Subsequently, the second-generation nanomedicines were developed with active targeting ligands on the surface to specifically bind to the receptors of targeted sites. Such receptors are overexpressed by cancerous tumor cells or tumor vasculature in contrast to normal, healthy cells. Moieties like antibodies, antibody fragments, aptamers, peptides and folic acid can all act as targeting ligands.[39-42] Many of this generation of nanomedicines are in preclinical or clinical trial status.[43-44]

2.2 Barriers inside the tumor

Once across the vascular endothelial cells, the restricted deep penetration of NPs in tumors poses a great challenge in the fight against cancer. Despite the large number of successful preclinical studies, many NPs have proven inefficient in the clinical environment due to their inability to penetrate deep within tumors – this is a result of the tumor microenvironment and the physico-chemical properties of the NPs themselves.[45-46] Figure 2 illustrates the main barriers to deep penetration which must be rationally considered when designing and engineering NPs in order to establish an efficient cancer treatment.

2.2.1 Heterogeneous vascular network

In comparison to normal vessels, tumor vessels are highly irregular and chaotic in structure.[47] The tumor vasculature network is dynamic in nature and varies from tumor to tumor; it sometimes even varies within the same tumor type at different stages of development. Consequently, the combination of these factors results in unequal permeability which, ultimately, constricts the distribution of delivered cancer therapeutics.[48]

2.2.2 Elevated interstitial fluid pressure (IFP)

IFP is a type of stress that is applied by fluids and uniformly elevated throughout tumors. Fluid flows through tumors via three main processes: flow along the tumor vessels; flow through the interstitial space, and drainage of any excess fluid by the lymphatic vessels. Consequently, any irregularities in the tumor microenvironment that regard any of these three processes lead to elevated IFP. For example, there is a lack of functional lymphatic vessels in tumors and this elevates IFP. An elevated IFP has the potential to disrupt the normal convective flow and thus it restricts the efficacy of NP transportation to tumor sites.[48] Furthermore, due to the stresses placed on vessel walls by the fluid, elevated IFP has the potential to compress tumor vessels and thus cause the vessels to collapse which, consequently, decreases the ability of the nanomedicine to be transported through the tumor vasculature. Additionally, elevated IFP might result in loss of interstitial fluid into surrounding normal tissues. As a consequence, this would result in transportation of both nanomedicine and tumor, thus spreading the malignant cells and increasing drug resistance.[47]

2.2.3 Stromal cells

Stromal cells provide structure, support and anchoring for all organs inside the human body. They resemble ligaments in that they are connective in nature.[49] In short, they are connective tissue cells. The most common types of stromal cells are cancer-associated fibroblasts (CAFs) and tumor-associated macrophages (TAMs). Studies have found that CAFs and TAMs can increase the rate of proliferation and metastasis of tumor cells. More importantly, they can negatively impact upon the transport and drug delivery of NPs by restricting their access to tumor cells.[48] According to Roode et al., despite the fact that TAMs only contribute about 1% of all cells in tumors, the attraction of NPs to TAMs is four-fold greater than that of cancer cells.[50] Additionally, the attraction of NPs to CAFs is approximately seven-fold greater than that of cancer cells. As a result, this off-target uptake of NPs by stromal cells decreases the uptake by cancer cells and, therefore, reduces the beneficial therapeutic effects.[47]

2.2.4 Dense extracellular matrix (ECM)

Within all tissues and organs there is a non-cellular component present called the ECM. It is formed by the secretion of components from both stromal and cancer cells and is comprised of two types of macromolecules: proteoglycans and fibrous-forming proteins.[51] Such proteins contribute towards the structure and function of the ECM which is constantly being remodeled, either enzymatically or non-enzymatically. Consequently, the ECM is a highly dynamic and complex network that stimulates tumor metastasis. Moreover, the dense ECM also prevents penetration and homogeneous distribution of the targeted nanomedicine in three significant ways. First of all, the restricted interstitial volume coupled with the high stromal cell fraction contributes towards a very dense network which, consequently, diminishes the blood flow and limits the convection of nanomedicines. Secondly, the diffusion of nanomedicines is limited by the collagen thickness, fibrillar structure and mesh size of the ECM. Matrix mesh sizes are typically within the range of 20-40 nm and thus only very small particles can achieve deep penetration; therefore, as many nanomedicines exceed this range they are prevented from diffusing through the ECM. Thirdly and finally, the tortuosity of the tumor interstitial space presents an additional barrier to the penetration of all drugs as the diffusion path that nanomedicines must travel along, from blood vessels to tumor cells, is elongated. Conclusively, dense ECM networks in tumors restrict the transportation of nanomedicines in both the vasculature and the tumor interstitial space.[47]

In order to overcome these four barriers and thus allow NPs to penetrate deep within tumors, requirements for NPs in this interstitial transport stage could be different from the previous two stages. From the compelling evidence generated by a number of independent groups, it has been confirmed that, in general, smaller and elongated NPs achieve greater tumor penetration than larger and spherical NPs.[48] And unlike vascular transport, positive charges facilitate the binding of NPs to inherently negatively-charged cell membranes and achieve deep penetration.[52-53]

3 Strategies for deep penetration

3.1 Dynamic regulation of the physico-chemical properties of NPs

As previously mentioned, the physico-chemical properties (e.g., size, shape, and surface chemistry in Figure 3) of NPs represent one factor towards determining the extent to which NPs can penetrate deep within tumor cells. However, an optimal physico-chemical property of a NP changes dramatically over time and place within the living body at different stages of transportation. The changing requirements of the properties of NPs at different transport stages have recently led to the growth of smart nanotechnology, where stimuli-responsive NPs can dynamically adapt in a surrounding tumor microenvironment or as a result of an external trigger.

3.1.1 Size/surface charge switch upon stimuli

Particle size plays an important role in determining how deep NPs can penetrate inside tumor cells. On the one hand, large particles, approximately 100 nm in size, boast advantages for high tumor accumulation in the leaky vasculature; on the other hand, they have poor penetration efficiency due to the large diffusion barrier in the tumor matrix.[48] Correspondingly, smaller particles are advantageous for deep penetration due to the presence of fewer diffusion barriers; nevertheless, they are prone to short blood circulation times and poor tumor accumulation rates as a result of rapid clearance.[54-56]

Surface charge is another influential property of nanomedicines for achieving deep penetration. However, the results from current research studies are mixed and sometimes contradictory. According to Jain & Stylianopoulos, neutral NPs diffuse faster and are distributed more evenly within tumors than their cationic or anionic counterparts, which is due to the fact that charged particles can form aggregates with oppositely-charged components in the same matrix.[24] In contrast, in a separate study, cationic lipidic NPs of around 100 nm were shown to achieve increased penetration in both three-dimensional (3D) tumor spheroids and in vivo tumor models than their anionic and neutral counterparts.[50] Meanwhile, Suzuki and Bae

suggested that the active penetration of the positively charged NPs is induced by iterative transcytosis.[53] However, one thing can be confirmed that negative NPs are not suitable for deep penetration, even in small concentration, they can form aggregates hindering penetration, while in an earlier study back in 2010, He et al. confirmed anionic (negatively charged) nanocarriers excelled in blood transport.[57]

A trade-off between these two purposes – tumor accumulation and deep penetration – exists for many NPs. However, it is desirable for NPs to exhibit both of these properties in order to maximize their drug delivery efficacy. Resultantly, such requirements have promoted the development of size-switchable or surface charge-switchable NPs which are able to maintain a large initial particle size and negative surface charge for long circulation time, and then responsively switch to a small size and positive or neutral surface charge for deep penetration and effective tumor distribution once they have accumulated at tumor sites.[58] Within these dynamic alteration studies, some NPs exhibit size change, with some causing a surface charge reversal. But most recently there have been increasing NPs able to exhibit a dual change, in other words, both the size and surface charge of NPs are able to undergo concurrent alterations in a multistage process. The size change can be achieved by some size shrinking materials or intratumoral release, and dual change is commonly achieved by the latter strategy. These switching events can be triggered by a number of stimuli, including internal stimuli such as pH, hypoxia andoverexpressed enzymes, and external stimuli such as light, ultrasound and temperature.[45] Figure 4 displays the different types of internal and external triggers.

pH:

The pH in the abnormal tumor microenvironment is mildly acidic (i.e. tumor extracellular pH, pHe), approximately between 6.5 and 7.0, which is lower than that in normal tissues and blood (≈7.4).[59] The pH value can further decrease to 4.5-6.0 in the lysosome/endosome (i.e. tumor cell intracellular pH, pHi).[60] Such a disparity in pH values can be utilized in order to trigger degradation of acid-cleavable linkers, or a polarity change of ionisable chemical groups. For

example, Dai et al. took advantage of two pH sensitive substances 2-propionic-3-methylmaleic anhydride (CDM) molecule and poly(2-(diethylamino) ethyl methacrylate (PDEA) to produce a size/charge dual changeable micelleplex for enhanced tumor penetration.[61] The acid-cleavable amide bond (pKa 6.8) from CDM provided the function of size shrinking at weak acidic tumor microenvironment pHe and then the ultra-pH-sensitive polymer, PDEA (pKa ≈ 6.4) core, was quickly protonated in pHi which provided the spiraling positive charge and triggered the release of cargos. As a result, the size of the micelleplex reduced from 111.7 to 43 nm, and its surface charge increased from 11 to 35 mV. When multicellular tumor spheroids (B16F10 cells) were incubated with micelleplex at pH 6.8 for 4 h, the fluorescence signal of micelleplexes in spheroids was 7-times higher than that of pH 7.4. Wang and colleagues constructed ultra-pH sensitive cluster nanobombs (SCNs) by linking small platinum prodrug-conjugated poly(amidoamine) (PAMAM) derivatives (PAMAM/Pt) particles to ultra-pH-sensitive PEG-PAEMA so that the amphiphilic polymer containing ionisable tertiary amine groups could facilitate rapid pH- responses.[62] Such superstructures had an initial size of 80 nm following IV injection; however, after accumulation in the tumor microenvironment, smaller NPs of less than 10 nm were generated (Figure 5A). Such size-switchable NPs showed significantly improved tumor penetration and drug delivery efficacy in comparison to pH-insensitive NPs that remained around 80 nm in size. Chen et al. designed and reported a shell-stacked NP (SNP) which could undergo both size and surface charge transformations.[63] Such a transformation was brought about by cleavage of dimethylmaleic anhydride (DMA) groups from methoxy poly(ethylene glycol)-block-poly(l-lysine) polymer in mildly acidic tumor microenvironments. As a result, the NP size was reduced from about 145 to 40 nm and the surface charge was reversed from -7.4 to +8.2 mV, which is a remarkable change (Figure 5B). In vivo investigations found that SNP penetrates about 1.1 mm inside the tumor mass (xenografted A549 lung carcinoma), which is about fourfold deeper than that achieved by its non-transformable counterpart. The recent work using a similar approach is illustrated in Table

1.

Overexpressed enzymes：

Matrix metalloproteinases (MMPs) are the main ECM enzymes in collagen degradation which occur in numerous different types of cancers.[64-67] Therefore, a strategy to trigger size-shrinkage of NPs can be based on the overexpression of MMPs, particularly MMP-2, in the tumor microenvironment. Gelatin is a substrate of MMP-2 and the enzyme degrades gelatin. With this principle, Wong et al. proposed a multistage system whereby gelatin NPs "shrank" in size from 100 to 10 nm after entering the tumor vasculature and being exposed to proteases such as MMP-2 due to the degradation of the cores NPs.[68] Moreover, Ruan et al. developed a similar construction of a kind of novel nanocarrier, G-AuNPs-DOX-PEG, which is a gelatin and gold composite NP loaded with DOX for enhanced tumor penetration.[69] Such a NP can be degraded by MMP-2 which causes the size to shrink from ~186 to ~59 nm. Thus, this type of NPs have been found to efficiently inhibit tumor growth in 4T1 and B16F10 tumor models in mice. Treating such tumor bearing mice with these NPs resulted in the lowest tumor growth rate. Consequently, size-shrinkable G-AuNPs-DOX-PEG are capable of exhibiting the best anti-tumor effect due to deep penetration of the NPs following by release of DOX.

Hyaluronidase (HAase) is another specific enzyme which is highly expressed in tumor microenvironment.[11, 70-71] Similar to MMP-2, HAase can cause the degradation of hyaluronic acid (HA) and then trigger the size shrinking of NPs whose shells are made by HA. Hu et al. presented hyaluronic acid (HA) shell based size-changeable intelligent NPs, DOX-DGL/ nitric oxide donor-modified hyaluronic acid (IDDHN).[72] After incubation with HAase for 4h, the size of IDDHN NPs shrank from 264 to 29 nm and the penetration depth of IDDHN NPs in 3D tumor spheroids can reach 80 μm (3.5-fold higher than that of NPs without HAase incubation). More recent size/surface charge switchable NPs upon overexpressed enzymes are listed in Table 2.

Hypoxia:

Hypoxia is a result of a low partial pressure of oxygen found in the deeper section of the tumor region where there is also an absence of blood vessels.[73-76] In order to target this region, NPs must be able to penetrate deep into the tumor microenvironment. One approach is to create NPs that are attracted to hypoxic cells within tumors. Similar to regular tumor cells, hypoxic cells contain overexpressed markers. Hypoxic cells are specifically overexpressed in phosphatidylserine which can be used as a target for delivery. Despite phosphatidylserine being found on the external membrane of cells where apoptosis occurs, it is also found on the endothelial cells of tumor cells. Hypoxic conditions increase the amount of phosphatidylserine, making it a prime marker to target. Wojton et al. found the addition of lysosomal protein Saposin C (SapC) onto NPs enhanced killing efficacy for hypoxic cells and increased survival.[77] This study used many models of brain cancers, including glioblastoma – the most aggressive forms of brain tumor. Hypoxia targeted delivery could be used with NPs with size change, surface charge change and controllable intracellular drug release. Hypoxia condition is able to trigger the cleavage of several hypoxia-sensitive moieties which can perform strong reductive reaction, such as azobenzene (Azo), or quinone derivatives, resulting in the properties switch of NPs.[78-79] Thambi et al. reported the synthesis of hypoxia-responsive NPs (HR-NPs). Under hypoxic conditions, the NPs would undergo a surface charge increase and hydrophobic-to-hydrophilic change via the reduction of 2- nitroimidazole to 2- aminoimidazole (Table 3).[80] The release of the hydrophobic drug DOX would occur in the internal hypoxic cells showing great targeting.

Light:

For photosensitive NPs, stimulation from light can be used. Light could come from ultraviolet (UV), visible and near infrared radiation (NIR) regions in the electromagnetic spectrum. Tong et al. designed spiropyran-based NPs being capable of shrinking from 103 to 49 nm upon exposure to UV irradiation at 365 nm due to photoisomerization.[81] When exposed to these

conditions, the hydrophobic spiropyran was converted to an amphiphilic derivative. Nevertheless, the use of UV-triggered size-switchable NPs has distinctive disadvantages including damage to healthy tissues, and limited ability to reach tumors in deep organs. As a result, NIR light or far infrared laser irradiation may be preferred over UV illumination as they result in increased tumor penetration and greater compatibility with biological systems. You et al. loaded DOX onto hollow gold NPs.[82] The study used NIR laser to achieve localized therapy. The energy from the light excites the NPs, forcing them to release the payload. Being hollow allows these particles to have an increased payload, one advantage over solid nanocarriers. The payload of DOX could constitute up to 60% of the weight of NPs. Ovarian cancer types Hey and A2780, as well as breast cancer cell MDA-MB-231 were tested with the same outcomes.

3.1.2 Size/surface charge switch upon multi-stimuli

Previous discussion on recent studies has highlighted multiple ways in which NPs may respond to the tumor microenvironment. There have also been examples on the requirements of the different stages and how these have been met in recent studies. A growing topic of research has become multi-responsive NPs. Having multiple triggers in a process could increase NPs' performance. Cun et al. produced a MMP-2 and pH dual triggered NPs, doxorubicin-conjugated dendrigraft-poly-L-(lysine)–EGPLGVRGK–poly(ethylene glycol)–poly(caprolactone) (DGL/DOX- EGPLGVRGK -PEG-PCL), which can achieve intratumoral degradation of NPs for twice.[83] The MMP-2 in tumor microenvironment caused the cleavage of PEG-PCL via EGPLGVRGK (a substrate peptide of MMP-2) hydrolysis that results in the first size shrink from 100 to 30 nm, and generated strong penetration of DGL/DOX in 3D in vitro model (Figure 6). The penetration depth of NPs can reach 80 μm after incubation with MMP-2 for 1h. Then, the acidic tumor intracellular environment triggered the second drug release to effectively kill tumor cells by breaking the pH sensitive hydrazine bond between the DGL and DOX.

Multiple-responsive NPs can also be built on redox environment. For example, the

concentration of GSH ranges between 2-10 mM in the tumor cells and 2-10 μM in the ECM.[84] This exceptionally large difference means redox triggering NPs is an effective way to induce a change of the nanocarrier.[85] One approach is to make use of disulfide bonds to control the properties and release of NPs. In ECM, disulfide bonds remain intact, while in the presence of reductive species, which are usually found in the tumor cells, the disulfide bonds break down. Using this principle, Sun et al. developed RGD-PEI-SS-PLA/PTX@MMP-2-sensitive nanoclusters. The MMP-2 cleavage peptide was first degraded and the disulfide bond between the PEI and PLA was only cleaved under intracellular high reductive condition (Figure 7).[86] As a result, the size of the nanocluster can be reduced from 200 to 30 nm in tumor environment and the redox-responsive property synergistically accelerate intracellular drug release to achieve favorable antitumor activity (Table 4). Addition of disulfide bonds can be implemented on many forms of nanocarrier including mesoporous silica NPs (MSNs), carbon nanotubes and PEGylation micelles which are just a few examples.[87-89]

Additionally, several studies were reported to engineer stimuli-responsive NPs using both internal and external triggers. Zhou et al. designed a MMP-2, light and temperature multi-responsive nano liposome.[90] The liposome is a temperature sensitive material containing MMP-2 cleavable PEG corona. An NIR laser sensitive photosensitizer, pheophorbide a (PPa), can produce mild-hyperthermia under NIR laser irradiation to trigger drug release. Through this, multiple functions like stable blood circulation, size shrinking and intracellular drug release were achieved in one system. The results showed that the PPa–GPLGLAG–PEG achieved 1.9-fold deeper penetration in 4T1 tumor spheroids compared with PPa-PEG (without MMP-2 sheddable ligands). Jiao et al. simultaneously used temperature and redox to trigger the properties change of MSNs.[91] The particles only exhibited drug release when the temperature was higher than 37 °C, suggesting that this technology effectively decreases risk of premature drug unloading as it would only occur under external stimuli. When the particles were in tumor cells, the presence of redox species coupled with the GSH in the nanocarrier, causes a rapid

cleavage of the disulfide bonds to release payload. Table 4 summarized recent examples of combinations of multiple stimulus to trigger size/surface charge along with their transition mechanism.

3.1.3 Shape switch

Except size change, the influence of NPs with different shapes on their penetration ability in tumor tissues has also been experimentally and theoretically studied. Most results confirmed the fact that rod-shaped NPs (including nanotubes and nanoworms) are preferable for tumor trans-vascular and interstitial penetration, while spherical and quasi-hemispherical NPs are good for subsequent uptake by cancer cells.[92-95] Therefore, it can be similarly imagined that shape switchable NPs will be advantaged for cancer treatment. However, this is rarely reported, possibly due to the difficult control.

Recently, Wang et al. reported a shape-changing micelle called HEKM which contained a MMP-2 responsive linker.[96] The shape transformation was triggered by the overexpression of MMP-2 in the tumor microenvironment. During blood circulation, the HEKMs were self-assembled as nanorods (diameter of 20 nm and length of 50-300 nm) for increased tumor targeting with the aid of a recognition element consisting of EGFR-HER2 targeting peptide and mitochondrial apoptotic peptide and enhanced internalization. Once HEKMs penetrated into the tumor matrix, their MMP-2 responsive linkers were sheared, resulting in shape transformation from rod to sphere (diameter of around 35 nm) for better uptake by cancer cells (Figure 8A-E). In additional to this strategy, pH sensitive cross-linking single polymer chains can provide another great opportunity to fabricate shape switchable NPs since they can mimic the reversible folding procedure of proteins and self-assemble into well-defined shape. Song et al. reported a single-chain tadpole polymer PDEA-b-P(OEGMA-co-PDS) (named SCTP), which performed controlled shape switch triggered by pH change.[97] At pH 7.4, SCTP was deprotonated to hydrophobic and self-aggregate into large (68.7 ± 2.8 nm) spheroid-like multi-tadpole assemblies (MTAs). Then at pH 6.9. MTAs were self-disassembled into smaller

(9.6 ± 0.3 nm) rod-like SCTP for deep penetration in tumor (Figure 8F).

Inspired by the self-regulation of conformation in response to biological signals of proteins, Ohta et al. designed a shape-shifting nanostructures using three different sizes of gold NPs as cores whose surfaces were decorated with folic acid as the targeting molecule and linked with DNA sequences to control shape switch.[98] Upon addition of an attaching strand (A1) and a detaching strand (L1comp), the assembled nanostructure will change to another shape (morphology 2) by reconfiguring the DNA assembly (Figure 9A, B). The targeting ligands folic acid were hidden in the morphology 1 and exposed on the surface in the morphology 2 (Figure 9C). The results showed that even without targeting molecules (folic acid), the cellular uptake (U87-MG cells) of morphology 2 was 1.5 times that of morphology 1. This strategy provides a new opportunity to develop future dynamic NPs which can be stable in blood travel and then transform into desirable shapes to overcome various biological barriers at disease sites.

3.1.4 Surface biochemistry

Apart from redesigning NPs size, shape and surface charge to optimize their transport and penetration kinetics, surface biochemistry as well as hydrophobicity can lead to the same effect. One of the advantages of NPs is the flexibility of surface modifications for properties control.[99] One way to improve the efficacy of drug delivery is to coat the surface with polyethylene glycol (PEG) – a process known as PEGylation. PEG coatings boast advantages for improved blood circulation, as they shield the surface from aggregation, opsonization, and phagocytosis. Hanes and colleagues discovered that large NPs coated in PEG are able to penetrate tumors that were previously considered impenetrable by uncoated particles if, and only if, they are densely coated.[100] Such densely coated particles can also rapidly diffuse within the tumor microenvironment and distribute evenly throughout the tumor – the effect of which is illustrated in Figure 10. Surface PEGylation of NPs minimizes the interactions between particles themselves and the tumor ECM due to the hydrophilic and uncharged nature of PEG, thus increasing their penetration in tumor tissues.[101]

The efficacy of NP drug delivery can be enhanced by decorating the surface of NPs with active targeting moieties. Chan et al. discovered that actively targeted NPs, within a 60 nm diameter range, accumulate 5 times faster and approximately 2-fold higher than their passive (non-targeted) counterparts; however, their penetration capabilities are significantly reduced.[102] This suggests that the tumor delivery efficiency and the subsequent tissue penetration can be conflicting. To achieve both efficient tumor accumulation and deep penetration, Ruoslahti discovered the advantageous effects of using a tumor-homing peptide, iRGD (sequence CRGDKGPDC).[103] The iRGD peptide follows a multi-step tumor targeting mechanism, and it can bind αvβ3/5 integrin and neuropilin-1 overexpressed on the cancer cellular membrane, which results in sufficiently deep tumor penetration; this is far greater than that achieved by conventional RGD peptides and their counterparts as they are only capable of transporting their drug payloads to the periphery of tumor vessels.

Moreover, cell-penetrating peptides (CPPs) and tumor-penetrating ligands have been widely used to facilitate the intratumoral penetration of NPs.[104] Hu et al. reported r9-S-S-DOPE (CN) nanovehicle based on the r9 CPPs (Sequence: rrrrrrrrrc-SH) which exhibited great penetration capacity to primary tumor mass and effective anti-lymph metastasis outcome in mice test.[105] However, for CPPs, non-specific interactions would be unavoidable and thus largely affect drug delivery efficacy in in vivo studies. Therefore, to overcome this problem, a "ligand presentation" strategy was developed, whereby the targeting ligands were shielded, thus preventing undesirable interactions from occurring. The targeting ligands can then be exposed in response to specific internal or external stimuli, such as those mentioned above in Section 3.1.1. For example, targeting ligands tend to be shielded by acidic detachable chemical groups (such as DMA connected molecules) to mask their cell penetrating function, or shown in the Figure 9, the "targeting ON/OFF" strategy.[98] Furthermore, more recent studies used tumor-penetrating peptides rather than CPPs, due to their targeting ability to tumor.[106] Kwon et al. used a cyclic tumor-penetrating peptide, LyP-1 (CGNKRTRGC) to decorate their NPs.[107]

Unlike CPPs, LyP-1 shows specific interaction with tumor by binding its cognate receptor (p32), which increased the tumoral accumulation by 20% and reduced the accumulation in organs, compared with non-LyP-1 NPs. Several recent and novel tumor-penetrating substances are summarized in Table 5.

3.2 Modulation of tumor microenvironment

3.2.1 Degradation of ECM

The tumor ECM is dense and comprised of collagen, fibronectin, hyaluronic acid, proteoglycans and stromal fibroblasts which act as barriers to deep penetration of NPs within tumor masses. As a result, degradation of the ECM can be considered a feasible approach to enhance tumor penetration of NPs.[58]

According to Zhang et al., losartan can be injected prior to NP drug delivery treatment in order to decrease the level of collagen I in tumors and thus facilitate deep penetration – the mechanism of which is illustrated in Figure 11.[108] Losartan pre-treatment of 4T1-bearing mice at 40mg/kg preceding IV injection of ~100 nm PEGylated liposomes resulted in a greater tumor distribution of liposomes and an increase of 22% of target site accumulation. A recent study reported the co-embedding losartan and anti-cancer drugs (DOX) into hollow mesoporous prussian blue NPs (HMPBs).[109] The drug losartan was released at the fixed point of the tumor tissue triggered by an NIR laser. The results illustrated that losartan can degrade the collagen I in ECM and triple the accumulation of DOX in tumor tissues (increase from 0.49% to 1.47% of the injected dose). Consequently, such studies confirmed that losartan has a penetrating-enhancing effect on NPs or co-delivered drugs. A most recent study proposed that using nitric oxide (NO), an endogenous free radical, can also degrade collagen in the ECM without introduction of toxic component.[110] The depletion mechanism was that NO has the ability to induce the activation of MMP-1 and -2, which can functionally disintegrate the tumor matrix collagen. In vivo study showed that NO treatment led to around 2-fold increase of DOX accumulation in tumors compared to saline treatment.

Furthermore, degradation of the ECM can also be achieved by functionalizing NPs with enzymes that degrade tumor ECM components. An example is coupling of hyaluronidase, which degrades hyaluronan – one of the main components of the ECM – to NP surface to enhance tumor penetration. The in vivo and in vitro studies carried out by Gong et al. in 4T1 tumor models illustrated that enzyme-modified NPs achieved significantly greater tumor penetration depths and thus overall drug delivery efficacy, in comparison with their hyaluronidase-absent counterparts.[111] Additionally, such coupling also reduced the IFP, thus further establishing uniform distribution of NPs inside tumor tissue.[58] This is particularly important in some types of tumors such as pancreatic ductal adenocarcinoma (PDAC).[112] This cancer has extremely low survival rate due to its nearly impenetrable ECM, and pancreatic stellate cells (PSCs) are the main culprit for this phenomenon. For better treatment, Han et al. reported that dual delivery of all-trans retinoic acid (ATRA, to trigger PSC quiescence) and heat shock protein 47 (HSP47 siRNA, a collagen-specific molecular chaperone for the regulation of ECM network) to PDAC via Au-NPs carriers induced effective reduction of ECM, correspondingly resulting in enhanced chemotherapy efficacy both for in vitro and in vivo tests.[112] In addition, as Zhang et al. reported, cyclopamine also showed the ability to modify the excessive desmoplastic ECM of PDAC.[113]

Moreover, as described above (Section 2.2.3), stromal cells in tumor microenvironment perform unwanted uptake of drug NPs and induce fibrosis that impede penetration of nanomedicines into deep cancer cells. Thus, targeting and depleting these matrix cells is also significant to the breakage of stromal delivery barrier and improve the intratumoral penetration of therapeutic NPs.[114-115] Many specific receptors expressed by stromal cells (e.g. FAP, FAK, FGFR and CXC-chemokine receptor 4) and strategies for targeted clearance of these stromal cells have been widely reported.[116-119] Ji et al. reported using amphiphilic peptide (C2KG2R9)-cholesterol self-assembled NPs loaded with DOX (PNP-D) and surface modified with mouse monoclonal antibody (mAb) to target and kill

CAFs.[120] This design fulfilled the aim of targeting, penetration and therapy. The mAb can specifically bind human fibroblast activation protein-α (FAP-α) which is selectively expressed by CAFs but not in normal cells.[121] The results of in vivo tests indicated that after treatment with PNP-D-mAb, the typical morphology of CAFs in mice tumors disappeared. The percentage of apoptotic cancer cells in PNP-D-mAb groups (60%) was much higher than that in the control (5%) and PNP-D (17%) groups. Miao et al. found that after repeated treatment with cisplatin, the expression of Wnt16 in CAFs was elevated, leading to drug resistance. In this case, anti-Wnt16 siRNAs was combined with NPs to target Wnt16 in fibroblasts to kill them.[122]

Except using chemicals or enzymes, the degradation of ECM can also be achieved by several external physical energy, for instance, ultrasounds, light and magnetic field (Table 6). Lee et al. applied a high intensity focused ultrasound (Pulsed-HIFU) to ECM-rich A549 tumor tissues. The results showed that it largely reduced the amount of collagen and hyaluronan in ECM, thereby the intensity of NPs in treated tumor tissues has increased 2.18-fold than that in untreated tissues.[123] .

3.2.2 Vascular normalization

The interaction between the disorganized vascular networks in tumors and the abnormal tumor microenvironment can result in increased IFP; consequently, this prevents adequate and homogeneous blood flow and, therefore, impedes deep penetration of NPs in tumors.[79] Therefore, normalization of tumor vasculature has become an increasingly popular method to improve the drug delivery efficacy of NPs. The process of vessel normalization transforms the abnormal phenotype of tumor vessels into those which resemble fully functional, cancer-free vessels; this is achieved by repairing the basement membrane, increasing the coverage of pericytes and thus decreasing the extravasation of the tumor vasculature. Doing so has the advantageous effect of lowering the IFP and thus increasing tumor blood flow, which significantly improves the rate of NP transfer within tumor vasculature. In tumors, many

proangiogenic molecules, such as vascular endothelial growth factor (VEGF), fibroblast growth factor (FGF), and platelet-derived growth factor (PDGF), are overexpressed, ultimately resulting in a chaotic tumor vessel structure to develop. Consequently, it is desirable to be able to block these proangiogenic signaling molecules in order to repair tumor vessels.[47]

Chanhan et al. showed that the delivery of small NPs (12 nm diameter) could be enhanced by repairing the abnormal tumor vessels in mammals.[124] This was achieved by blocking VEGF receptor-2 with an antibody, DC101. Nevertheless, such a procedure only enhanced tumor penetration of NPs with 12 nm in diameter and the larger NPs (125 nm diameter) could not benefit from this approach.[45] This was due to the fact that DC101 decreases tumor vessel pore size and thus reduces IFP, which facilitates the convective permeation of small NPs and hinders the extravasation of larger NPs. Conclusively, such results further emphasize the fact that smaller NPs tend to achieve greater drug delivery efficacy and, therefore, are considered more efficient cancer treatments due to their ability to reach greater tumor penetration depths.[124]

Cyclooxygenase-2 (COX-2) is highly expressed at the tumor regions and it is actively involved in diverse cancer types for dense ECM formation and angiogenesis.[125] Thus, applying COX-2 inhibitors could be an effective tool to normalize tumor microenvironment including both ECM damage and vascular normalization functions. Kim et al. reported indomethacin (IMC) can produce effective angiogenesis inhibition via COX-2 blockade.[126] Zhang et al. reported a COX-2 inhibitor, Celecoxib, to disrupt ECM and reduce tumor-associated fibroblast and normalize tumor vessel on A549 tumor xenografts (Figure 12).[127]

3.2.3 Vascular disruption

Intratumoral transport of NPs can be improved by enhancing the permeability of tumor vessels, i.e. transvascular transport; this varies significantly between different tumors and is heterogeneous within the same type of tumor and at the same stage of development. The permeability of tumor vasculature consists of two stages: a dynamic event of vascular bursts

succeeded by a brief eruption of fluid into the tumor interstitial space. Smaller NPs (30 nm) are more easily distributed throughout the tumor as they can utilize both the eruption and static permeability stages, whereas larger particles rely on the dynamic eruption alone.[48]

As a consequence, vascular disruption can be achieved by pre-treatment with vascular disrupting agents (VDA), or radiation, ultrasound, and NIR laser irradiation, in order to enhance the permeability of tumor vasculature and thus improve intratumoral transport of NPs.[128-130] CA4P is a potent VDA which can cause endothelial damage by elevated serotonin and nitric oxide (NO) production. Studies have shown that greater tumor penetration depths are reached by NPs conjugated with CA4P. Satterlee et al. investigated and documented that co-injection of CA4P with lipid-platinum-chloride NPs led to accumulation of NPs in tumor vessels in mice.[131] They observed a clear vascular disruption effect in UMUC3/3T3 and 4T1 tumors, and target NP accumulations increased from ~1.2 to 2.1 injected dose%/gram and from ~2.5 to 3.2 injected dose%/gram for the two models, respectively. Such a study, amongst many others, strongly supports the fact that VDA are capable of enhancing the permeability of tumor vessels and the tumor penetration depths reached by NPs. However, the efficacy of VDA is compromised by their toxicity and the side effects that they can cause. Nonetheless, physical encapsulation or chemical conjugation of VDA in nanocarriers has the potential to overcome these negative effects and thus increase their clinical potential.[45]

Theek et al. showed one example of using ultrasound to induce vascular disruption and improve the penetration of 133-nm liposomes[132] Microbubbles were injected with liposomes at the same time, under the effect of ultrasound, the oscillation produced by microbubbles can open the tight junctions in vascular endothelium (sonoporation). Upon sonoporation, the relatively large liposomes (above 100 nm) can also cross out of the blood vessels and penetrate into the tumor interstitium, and around 60% of liposomes were found in the 10 μm region surrounding the vascular wall and around 20% of them reached 50 μm from the vessels.

Moreover, the transforming growth factor-β (TGF-β) is a multifunctional cytokine and

plays a role in the ECM production, angiogenesis and metastasis.[133] Several TGF- β inhibitors (TGF-β-I) have been proved to prevent some cancers from metastasizing.[134] Moreover, their functions to improve vascular permeability were also been explored. Cabral et.al reported that the TGF- β inhibitor can lessen the pericyte coverage of the tumor endothelial wall and increase the penetration of NPs.[135] They first compared the penetration properties of 30 nm and 70 nm micelles in mice BxPC3 xenografts. At 1 h post-injection, the 30 nm micelles had been apparently observed in cancer cells that are 40 μm from blood vessels while the 70 nm micelles still remained near the vasculature without further penetration to the interstitial space. This results reflected that size is a pivotal characterization to govern the tumor penetration of NPs. However, when the mice in the 70 nm micells group were pre-treated by a low dose (1 mg/Kg) of TGF-β-I (LY364947), the results became completely different. The tissue penetration ability of 70 nm micelles was augmented to a similar level compared with that of 30 nm micelles. At 24 h post-injection, both of them were detected at 100 μm from the blood vessel and displayed comparable subcellular localization.

In conclusion, vascular disruption can be utilized in order to enhance tumor vessel permeability and thus improve NP penetration within tumor tissues. On the other hand, vascular normalization can increase blood perfusion and lower the IFP, which consequently promotes convective diffusion of NPs in tumor tissues. Nevertheless, vessel pore size can be reduced by such a strategy which hinders the penetration of larger NPs. As a result, the tumor vasculature should be carefully monitored and regulated in order to achieve an optimal balance which enhances tumor vascular permeability and blood perfusion, thus promoting intratumoral NP transport.

3.2.4 Hypoxic normalization

The hypoxia region located in the deep tumor is absent of blood vessels.[136-138] Eventually it reduced penetration of systemically administered nanomedicines to this region. In addition, hypoxia triggers significant genomic and proteomic changes in cancer cells, and thus, it is

central to tumor growth, metastasis and treatment.[139] Increasing the oxygen concentration in hypoxic region is crucial for the diffusion of NPs in solid tumors.

One view is that hypoxia is associated with the active activity of mitochondria-associated oxidative phosphorylation (OXPHOS). Xia et al. reported gelatin-based NPs containing FDA (U.S. Food and Drug Administration) approved OXPHOS inhibitory drug, atovaquone (Ato), to transform hypoxia to normoxia. The NPs exhibited size shrinking (from 437 to 14 nm) under tumor microenvironment observation because of the degradation of gelatin coating by MMP-2 enzyme and followed release of Ato in the deeply hypoxia regions.[140] Other OXPHOS inhibitory drugs have also been reported including metformin and papaverine.[141-142] Another view proposed by Milotti et al. is that the shortage of oxygen concentration in tumor could be largely due to the low-frequency oscillations of arterial circulation,[143] while they found that a type of antihypertensive drug, alpha-blockers, can reduce or even abolish this low-frequency rhythms and result in enhanced diffusion of oxygen in solid tumor.

Moreover, Chlorine e6 (Ce6) is a kind of photosensitizer, used for fluorescence imaging, but it can generate singlet oxygen ($^1O2$) when it is activated by light.[144-145] Min et al. attached Ce6 to the gemcitabine (GEM) eluting polyurethane (PU) membrane.[146] After exposure to 671 nm laser at 80 J/cm^2, the tissue penetration efficiency of GEM increased 2-fold and the tumor volumes in Ce6–GEM–PU + light group is 3-fold smaller than that in the group treated with Ce6–GEM–PU but without light exposure. Qian et al. reported a new photosensitive moiety as well as NIR imaging agent, dithiophene-benzotriazole, which can also produce $^1O2$ under the activation of visible/near-infrared (Vis/NIR) light.[147] Then they combined it with the 2-nitroimidazole to perform subsequent drug release in hypoxic cells (Table 6). Some proteins, such as human ferritin nanocages (FTn), were reported to have intrinsic ability to penetrate to the hypoxic region of tumor.[148] To enhance the colloidal stability of FTn, Huang et al. engineered a unique spatially controlled PEG coating to FTn (PEG-FTn$^{75\%}$) instead of conventional whole-covering PEGylation strategy.[149] The hybrid PEG-FTn75% can make sure

the exposure of FTn and resulted in the capable of delivering chemotherapeutic drugs to the hypoxic lung tumor tissues in vivo (Figure 13a). At the 18 h after the administration, the amount of PEG-FTn$^{75\%}$ found in hypoxic tumor regions was significantly higher than that of non-PEGylated FTn (Figure 13b, c).

3.3 Magnetic field for deep penetration

Tumor hypoxic regions show high resistance to the pharmaceutical nanocarriers penetration and to radio or laser beams spread.[150] Thus, beyond the addition of anti-hypoxia drugs to nanosystems, extra external propelling forces, such as magnetic and acoustic forces, are widely considered to promote the penetration of nanomedicines to deep hypoxic cancer cells.[151] Among them, the magnetic force occupies the incomparable position since its spread is barely affected by hypoxic regions and its low toxicity. Magnetic NPs (MNPs) have been approved for the clinical use for the generation of hyperthermia to control drug release under dynamic magnetic field, for example, NanoTherm®. Moreover, there is a strong preliminary evidence indicating that the external magnetic field can direct the delivery of drug-loaded MNPs to tumor sites.[152-154] Thus, recently, magnetic fields including static magnetic field and dynamic magnetic field with corresponding MNPs are gaining popularity in assistance of nanomedicines for tumor deep penetration.

For deep penetration, MNPs must show high magnetic saturation, biocompatibility and biodegradability. Commonly used MNPs are superparamagnetic iron oxide (Fe_3O_4 and MFe_2O_4 (M=Mn, Co and Zn)) which are widely existing in microorganism (bacteria and fungus) and can be synthesized in the laboratory. For example, Felfoul et al. used magnetotactic bacteria, MC-1 (naturally contains a chain of magnetic iron-oxide nanocrystals), as the drug carrier.[155] The results showed that more than half of MC-1 cells have crossed peritumoral regions and penetrated into hypoxic regions of colorectal xenografts under a directional three-dimensional magnetic field. Guo et al. examined the penetration depth of different sized Fe_3O_4 NPs (60, 120, 200 and 310 nm) in multicellular tumor spheroids, the results are 83.5, 69.7, 42.6 and 35.6 μm,

respectively.[156] Shamsi et al. constructed a computational model for numerical evaluation of the interstitial penetration efficiency of drug-loaded MNPs (200 nm) in the medium (R = 5 mm) and large (R = 10 mm) sized peritoneal neoplasms against dense ECM and high IFP (Figure 14A,B).[157] It was believed that the magnet strength and the distance between tumor and magnet are critical for successful penetration of MNPs in large tumors while there is less concern in small tumors.

In addition to strong rare earth magnets and electromagnets, the primary sources of external magnetic fields, magnetic resonance imaging (MRI) scanner was reported to be an alternative magnetic field generator for MNPs directing by Muthana et al.[158] Each MRI scanner contains inherent magnetic field coils, but the magnetic field is homogeneous without orientated propelling function. Hence, in this study, they supplied a 300 mT m^{-1} gradient coil to the 7 T MRI system to generate substantial actuation forces on MNPs loaded macrophages. They investigated its efficiency in a novel transendothelial migration flow model (Figure 14C). The results indicated that this magnetic field gradient (MRT) can steer magnetic macrophages across vascular endothelial layer against the blood flow shear force and fully penetrate into human multicellular tumor spheroids after 1h application (Figure 14D). The success of this study is meaningful because MRI is also a significant tool to diagnose and image cancer. It provided an opportunity for concomitant imaging and therapy of tumor.

Except being used as this navigation strategy, Schuerle et al. provided a novel approach to utilize the magnetic attraction between magnetic fields and MNPs for achieving deep penetration of nanomedicines.[159] Without the help of external forces, the convection and diffusion are two main approaches that NPs were used to penetrate within the tumor. Thus, they engineered two types of magnetic micropropellers powered by rotating magnetic fields (RMFs) to enhance diffusive transport of NPs. The one is natural magnetotactic bacteria (MTB) and the other one is magnetic artificial bacterial flagellum (ABF). Under the influence of a rotating magnetic field (continuous magnetic torque power), both micropropellers performed forward

propulsion and increased convective flow in the surrounding fluid in a microfluidic model. More importantly, these magnetic micropropellers are compatible with a wide range of NPs because the method just required simple mixing magnetic NPs and medicine NPs.[159]

3.4 Biological and biomimetic nanocarriers for deep penetration

Apart from using diverse laboratory-made functionalized organic, inorganic and polymeric NPs, some naturally occurring viruses and cells can exhibit intrinsic tissue penetrated properties.[160-161] The natural mission of animal virion NPs is to deliver their genes and accessory proteins into potential host cells. Viral protein transduction domains (e.g. 11–amino acid protein form HIV Tat) enable them to achieve a series of delivery activities in host cells, including penetration of mucus layers, fast cellular membrane attachment, endocytic entry, efficient tissue penetration and final nuclear import.[162-163] It is worth noting that for viruses, acidic pH (pH 6-6.5) in endosomes is an essential trigger for penetration and uncoating (release of viral genomes).[164] This trigger condition exactly matches with the acidic tumor microenvironment. Besides, some immune cells are able to migrate across impermeable barriers and unload their cargo at infected sites.[165] For instance, neutrophils (NEs), the most common type of immunocytes, have been widely used in brain-targeted drug delivery because of their native abilities to cross the blood–brain barrier (BBB) and penetrate glioma.[166-167] Thus, the biological or biomimetic nanocarriers may surpass other nanocarriers in some tumor types and be a breakthrough to deliver cargos to deeper cancer cells.

Zhang et al. produced virion-like NPs, 2, 3-dimethylmaleic anhydride decorated tumor-activated arginine-rich dendritic peptide prodrug (DA-Dend- R4K2K- Hyd-DOX） NPs (average size of 136.3 ± 5.8 nm), which mimicked both the natural protein transduction domains and dendritic arginine-rich virus-like architecture to acquire intrinsic multivalent effect to increase tissue and cell dual-penetration.[168] After confirming that virion-like NPs can recognize the tumor-specific acidic pH microenvironment in a biomimetic biphasic model system, they did penetration measurement in a special in vitro model by uniformly seeding

SKOV3/R cancer cells in 3D μ-slide chamber with matrigel to ensure the incubated conditions much closer to the real tumor microenvironment. The confocal fluorescence microscopy images showed that the viron-like NPs penetrated more than 600 μm. Xue et al. used NEs as the drug carriers to encapsulate paclitaxel loaded liposomes (PTX-CL/NEs).[167] The inflammatory factors (interleukin-8 and tumor necrosis factor) can direct the movement of PTX-CL/NEs toward brain tumor. The results of mice treatment showed that the PTX-CL/NEs treatment increased the 50% survival rate of up to 61 days, while this value for PTX-CL treatment was only 38 days.

4. Discussion

4.1. Advantages and disadvantages of different strategies for deep penetration of nanomedicines

The use of nanotechnologies to target tumors with deep penetration depth for efficient cancer treatment has been a main source of attention for researchers in recent years. This is a result of their potential ability to overcome several limitations related to conventional chemotherapeutic drug formulations. They offer: (1) enhanced drug loading capabilities, (2) ability to protect enclosed drug molecules from physiological hazards, (3) ease of adaptability to passive and active targeting, (4) multi-functionalization, and (5) improved biocompatibility. Consequently, it comes as no surprise that nanomedicine is regarded as a fast growing area of research in the world.

However, in the context of clinical cancer therapy, due to the biological barriers of tumors, these nanomedicines are usually accumulated at the invasive edge of the tumor, with inability for further penetration, so the tumor cells loaded in the necrotic inner layers of tumor are often untreated and cause, causing tumor recurrence. Thus, the most difficult barrier that nanomedicine engineers need to overcome is that of achieving great tumor penetration depths. To address this, nanomedicines are designed to facilitate tumor interstitial transport, such as reducing particles size, regulating particles shape and decorating the particle surface. While this

caused a following problem since the requirement in each transport stage is different. The above design does increase the penetration depth, but at the expense of pharmacokinetics, limiting their accumulation at tumor sites. As a consequence, in order to overcome such a problem, four significant options exist: dynamic fine-tune the physico-chemical properties of NPs, remodel the tumor microenvironment, use external sources of energy (e.g., magnetic force), or adopt biological and biomimetic nanocarriers.

These strategies can be further broken down into more precise categories. In the context of dynamic fine-tuning the physico-chemical properties of NPs, this can be done through intratumoral regulation of particle size, shape and/or surface biochemistry. Modifying each of these properties individually has a significant effect on the resulting penetration depth achieved by NPs within tumors; however, this effect can be further increased by optimizing such properties concurrently. NPs can be engineered in such a way that these properties can undergo changes triggered by internal or external stimuli, including pH, overexpression of enzymes, redox, hypoxia, light, ultrasound and temperature. Such a feature is highly desirable for NPs as it enables them to exhibit multiple properties which, consequently, allows for maximum drug delivery efficacy to be achieved. Resultantly, stable, programmed NPs circulating in the blood are activated upon arrival at the specific tumor site and thus are able to reach greater penetration depths. In addition to the control of above features, tuning the membrane rigidity was reported to be a potent strategy for improving the tumor penetration ability of liposomal NPs. Yuki et al. quantitatively demonstrated the rigidity (bending modulus (Kc)) of liposomes and they found there is a positive correlation between the rigidity and permeability of liposomes in the solid tumor.[169] In a recent study, Zhang et al. illustrated the huge influence of NPs surface architecture on intratumoral penetration.[170]

Except controlling the properties of NPs for deep penetration, the tumor microenvironment can be remodeled in a number of ways, including degradation of ECM, vascular normalization, and vascular disruption via pharmacological or physical strategies.

Vascular normalization can increase blood perfusion and lower the IFP which promotes convective diffusion of NPs in tumor tissues. On the other hand, vascular disruption can enhance tumor vessel permeability and thus improve NP penetration within tumor tissues. Thus, an optimal balance which enhances tumor vascular permeability and blood perfusion should be better determined. For example, the normalization of tumor vessels may cause the compromise with the EPR effect. Conclusively, the tumor vasculature modulation requires careful monitoring and regulation in order to achieve deep penetration of NPs.

Overall, the above two strategies have promoted tumor penetration of nanomedicines to varying degrees and improved therapeutic efficacy, but they are still associated with several problems, which restrict their further clinical development. For the strategies of internal triggers induced NPs properties change and modulation of tumor microenvironment, one limitation should be highlighted is the heterogeneity associated with tumor growth. It can vary between different tumor types, individual patients, of course, would differ greatly between species. Mouse tumors, although grown with humans in mind, would exhibit size and growth variations. This certainly raises a question into current research in these two strategies because their effects are highly influenced by tumoral types and patients. Proven techniques in mice are probably not successful in humans. Another disadvantage is that the design and synthesis of this kind of smart NPs are relatively complex, requiring elegant control of the physico-chemical properties of NPs under different conditions. In contrast, for external triggers induced properties change, such as laser radiation beams and ultrasound, their treatments less lie with the heterogeneity of the tumors between patients, and thus they are more likely to achieve clinical translation. Their significant disadvantages are their responses would be largely reduced in tumor avascular zones (oxygen free) and their working areas are rather localized. They cannot administer tumor systemically and show limited therapeutic efficacy for metastasized lesions. However, the advantage of the approaches in this category is that they minimize the disruption to patients' biological system. In great comparison, degradation of the ECM has a potential shortage that it

may stimulate the movement of tumor cells, and result in cancer metastasis. This situation could be explained that degrading the dense ECM will break the collagen network and cell-matrix combination, thus causing the bidirectional penetration of the cancer cells. In other words, while damaged ECM makes nanomedicines easier to penetrate, it facilitates the leaking out of the surviving tumor cells from the vascular endothelium (endothelial leakiness) meanwhile, thus cancelling out the treatment effects. One example was reported by Peng et al. in this year.[171] Therefore, special consideration should be given to the strategies that remodel the tumor microenvironment for enhanced drug delivery.

Based on these problems, supplemented strategies that use magnetic pulling force or intrinsic tissue penetrated properties of viruses and cells to increase nanomedicines penetration depth have been reported. Particularly, magnetic force has been widely investigated recently for three reasons. First, the oxygen-free condition will not affect the spread of magnetic force, and it could exhibit great outcomes in vivo because it is independent of heterogeneous between different tumors and patients, and pathological properties of tumors. Second, compared with laser beams manipulation, magnetic field shows less damage to healthy cells. Third, it has the potential to treat metastatic tumors because MNPs can be injected systemically. Muthana et al. have shown their magnetic system can target both primary and secondary metastatic tumors in mice test.[158] However, the question of this strategy is that whether the magnetic force is sufficient to allow drug-loaded MNPs to perform interstitial transport and whether it will aggravate tumor local heterogeneous resistance. And to clinical translation, the ability to provide the same magnetic propelling force to human is still being studied.

4.2. Integration of different strategies for improved outcome

Each of the above described penetration strategies boasts its own advantages and disadvantages for different applications and, therefore, further research is required into the specifics of each one. For the same reason, as discussed in our previous review, a natural design is to combine different strategies together to maximize the outcome and minimize the negative

effect.[172] Many researches have been reported and some recent examples are listed in Table 7.

Additionally, the improvement of penetration of NPs in tumor tissues is not only good for enhancing cancer treatment efficacy but also useful for tumor imaging and diagnosis.[173-175] Zhou et al. created multi-responsive nanocarriers for treatment of triple-negative breast cancer.[90] The NPs decreased the size in the tumor microenvironment through contacting with MMP-2. Pheophorbide a (PPa) caused mild-hyperthermia with NIR radiation and it also enabled the NPs to be suitable for imaging. In the meantime, the NPs induced reactive oxygen species (ROS) generation to aid photodynamic therapy (PDT). Overall, these NPs are enzyme, light and heat sensitive with imaging capacity. Qian et al. designed a smart multi-peptides functionalized nano delivery system named as STD Nano-micelle (NM_{drug}).[176] This delivery system contained five functional elements for the simultaneous achievement of cancer diagnosis, tumor targeting therapy and enhanced tumor penetration. In brief, the five components are peptide STP (sequence: SKDEEWHKNNFPLSPG) for pH-triggered target, a caspase-3 triggered peptide linker (sequence: DEVD), TPE (tetraphenylethylene) which exhibits 'switch on' fluorescence during apoptosis, cell-penetrating peptides TAT and DA (2,3-dimethylmaleic anhydride) for shielding the cation on TAT. As a result, the STD-NM performed in a stealth state in the blood circulation because of the DA, and then only in the tumor site, the STD-NM could be switched to the activated state. The acidic pH stimulated STP and TAT for enhanced cell permeability and caspase-3 stimulated DEVD and TPE for fluorescence imaging of cancer cells (Figure 15).

Wang et al. reported a complex therapeutic nanoplatform, ATLP, which took advantage of three strategies (size shrinking, surface chemistry and ROS generation) and both internal and external stimuli for the tumor-targeted deep penetration.[177] The ATLP NPs consisted of a Ce6 modified PEG-b-poly(2-(hexamethyleneimino) ethyl methacrylate) shell (termed as PHMA) and an amphiphilic iRGD-GALGLP-P85-PLGLAG-DOX core (termed as iPAPD). First, in the tumor microenvironment, the ultra-acidic-sensitive PHMA performed a property transition

from amphiphilic to hydrophilic resulting in its detachment from iPAPD. As a result, the iRGD and Ce6 were exposed to facilitate tumor-targeted penetration and real-time fluorescence imaging, respectively. The fluorescence signal of NPs at pH 6.6 is 3.4 times higher than that at pH 7.4 (Figure 16A). Second, the MMP-2 enzymes triggered further intratumoral drug release of DOX via the cleavage of MMP-2-labile peptide, PLGLAG. Third, the external stimulus, NIR laser was employed to enhance intratumoral DOX diffusion by inducing Ce6 (also a photosensitizer) to produce ROS inside tumor. The results showed that the intratumoral DOX accumulation in iPAPD groups is 3.5-fold higher than that in free DOX groups (Figure 16B) and iPAPD + laser treatment completely eliminate the mice tumor xenograft (Figure 16C). As a result, this study provided an effective approach to combine multi strategies into one nanoplatform and fulfilled the purpose of theranostics simultaneously. More recent examples are summarized in Table 8.

So far, since extensive researches have been studied in using these individual approaches and their combinations for cancer treatment and imaging in animal models and promising outcomes have been achieved. With these findings as the basis, future research should be directed towards improving the clinical relevance and translational feasibility of these technologies, which is also the ultimate challenge of nanotechnologies in tumor deep penetration application. NPs that prove successful in vivo testing on animals hardly reaches the same conclusions in humans, and post successful trials NPs must be able to be reproducible, scalable and manufactural for worthwhile commercialization. Simpler, one-stage NPs could possibly be made with current pharmacology unit operations, while the much more complex NPs described throughout this review will require innovative techniques, consequently adding years to their mass productions and public release.

4.3. How deep is deep?

As of June 2019, using '(nanoparticles/liposomes/micelles) AND (cancer/tumor)' as the search words will yield 71,141 publications on Web of Science, while this number will dramatically

decrease to 2675 when adding an extra keyword 'penetration'. The results reflected the fact that, for decades, around 95 percent of researches on nanomedicines was focused on increasing accumulation of free drugs to tumor sites by taking advantage of nano size (first- and second-generation NPs), but often few of them have looked at further tumor tissue penetration improvement. Therefore, at present, the production of penetration facilitated NPs (third-generation NPs) can be considered as a proof-of-concept study, and which is still staying in the laboratory test phase. To determine its future pathway, the progress that the current researches have carried out should be rigorously investigated.

To prove the validity of these NPs in tumor penetration, their depth-of-penetration should be evaluated as an important parameter. For the assessment of NPs penetration in vitro, a significant mass of studies chose cancer cell-seeded collagen scaffold, 3D tumor multicellular spheroids and microfluidic tumor model rather than monolayer cells.[178-180] This is because these models can better simulate the real transport conditions in tumor extracellular matrix and tumor microenvironment.[181] Tumor spheroids are able to form specific penetration barriers (e.g. hypoxia, proliferative gradients and control of certain ECM components) when their sizes beyond 350 μm.[182] The microfluidic tumor model is an upgraded model that supplies the simulation of endothelial cellular layer, local tissue-tissue interfaces and blood flow to test the targeting, extravasation efficacy and penetration of NPs against blood flow shear force or interstitial flow, some examples mentioned above.[183-184]

For in vivo evaluation, xenograft mice tumor models have been frequently used. The penetration depth of NPs in the mice models is a crucial datum to predicate their clinical performance. As displayed in Figure 17, 21 publications were found to have quantitative data of the penetration depth of NPs from the tumor vessel (intravenous injection). The used penetration strategies in these publications include size/charge switch, surface chemistry decoration, modulation of tumor microenvironment, ROS generation and biological delivery (single use or combination of more than one strategy). The maximum penetration depth is 480

μm in colon tumor via the combined strategy of size reduction and ROS generation and the work was published in 2019.[185] However, in most of the work, the penetration of NPs is below 200 μm. The mean and median of penetration depth of the evaluated penetration depth is approximately 130 and 90 μm, respectively. When the penetration depth is measured from the tumor periphery, the values can reach up to 2 millimetre level in some studies.[63, 186-187] One novel strategy was using repeated intra-intercellular delivery for enhanced penetration of DOX.[186] This was achieved by the construction of monostearate protected DOX preloaded amorphous calcium carbonat (MS/ACC–DOX) NPs. The high aqueous instable amorphous calcium carbonat (ACC) NPs can achieve burst release of DOX in cancer cells, and after inducing death of one cell, they can move to the next cell and repeat the drug release process, like peeling an onion layer by layer (Figure 18). This strategy allows the loaded drugs to have more chances to reach the cells near the tumor core. However, if comparing this penetration depth with the real size of many tumor tissues, it is apparently insufficient.

As a result, it can be expected that fulfilling the whole tumor penetration in the human body will not be an easy goal, based on current data. Besides, although researchers have testified their multifarious strategies can improve the penetration of NPs or drugs in in vitro or in vivo models at varying degrees, their outcomes in clinical setting remain to be determined. For example, the size, stage and location of tumor and the specific barriers for different tumor types and individuals are different. All of these factors could have an outsized impact on the behaviour of NPs in thebody. It is often that the design of NPs for deep penetration is complex, imposing great difficulty in obtaining approval.

4.4. Potential of immunotherapy to boost the effect of nanotherapeutics

As described above, the tumor penetration facilitated NPs seem to have a bleak prospect in killing all tumor cells. In this circumstance, the future direction of nanomedicines needs to be carefully rethought beyond simply aiming for deeper and deeper penetration depth. For example, the strategy could shift to excite the immune system (i.e. immunotherapy) by reasonably

improved penetration. In fact, the immunotherapy and deep penetration NPs could build a mutually beneficial relationship by two strategies.

First, using nanocarriers to establish a 'specific-drug reservoir' in the vicinity of the tumor matrix and kill some tumor cells. It could be sufficient to induce immunogenic cell death (tumor immunity) and then the T cells, especially cytotoxic $CD8^+$ T lymphocytes (CTLs) can kill inner chemotherapy-resistant cancer cells (Figure 19).[188] Thus, in this case, penetrating whole tumor tissues is not always needed. Krysko et al. pointed out that the ability of a cancer therapy to produce ROS and endoplasmic reticulum (ER) stress (either in parallel or in tandem) determines whether it can induce immunogenic cell death.[189]

Second, delivery of cytotoxic T lymphocyte protein 4 (CTLA4) inhibitors or programmed death-ligand 1(PD-L1) inhibitors to the tumor sites is an alternative strategy to initiate antitumor immune response via the break of tumoral adaptive immune response or immune evasion.[188] Apart from innate immune cells (e.g. macrophages, dendritic cells and neutrophils) in the tumor microenvironment, T cells (i.e. T and B lymphocytes) take the main responsibility of suppression and control of tumor growth.[190] But tumor seems like a 'clever' organism which can develop the self-protecting mechanism to against their attacks.[191] CLTA-4, as well as PD-L1 and its receptors (programmed cell death protein 1, PD-1) are significant immune checkpoint molecules in the associated process. For example, many tumors will overexpress PD-L1 to specifically bind PD-1 which expressed on the surface of T cells and then induce the apoptosis of T cells. In this case, using PD-L1 or CTLA inhibitors to stop the resistance of tumor seems to necessary and promote T cell priming, and the tumor regression effect of this checkpoint blockade therapy has been proved in a range of malignant tumors (e.g. lung, ovarian, bladder, melanoma and colorectal cancer) and many immune checkpoint inhibitors have been approved by FDA.[192-193] Therefore, consideration of adding these components into the design of NPs could be a promising way as only tiny tumor penetration depth is possible to be achieved until today.[194-196] Dai et al. used the above two strategies,

photodynamic therapy (ROS generation) and PD-L1 gene silencing, with deep penetration NPs for cancer treatment.[61] PD-L1-blockade siRNA (siPD-L1) and a photosensitizer, MTPP (5-(3-Hydroxy-p-(4-trimethylammonium)butoxyphenyl)-10, 15, 20-triphenylporphyrin chlorine) were encapsulated into the size and charge changeable pH-responsive micelleplex (denoted as PCPP). PCPP protected the drugs during blood circulation and its property change ensured siPD-L1 and MTPP to penetrate to a considerable depth in the tumor microenvironment. At 2 h post-injection into the B16F10 tumor-bearing mice, PCPP@MTPP@siPD-L1 could be detected at a tumor depth at 300 μm. Then the highly positively charged PCPP were disintegrated in the pHi to release the cargos. The results showed that after cargo release, the level of $CD8^+$ T cells and helper $CD4^+$ T cells in tumor had a 10-fold and 7-fold increase, indicating successful activation of immune response in vivo. In the following antitumor test, the PCPP@MTPP@siPD-L1 + irradiation group can eliminate almost all tumors (via tumor volume analysis) after treatment for 18 days, and the survive rate was 83% after 30 days. Moreover, the activated immune effect largely decreased the tumor recurrence rate from 100% (control and PCPP@MTPP groups) to 25% after 28 days.

5. Conclusion

In conclusion, nanomedicine represents one of the fastest growing research areas and is considered to be one promising therapy for treating cancer with deep penetration. This review has highlighted the delivery problems associated with nanotechnology, which is partially hindering the translation of nanomedicine in clinical cancer treatment. Several strategies to balance all of the requirements of drug transport in blood circulation, tumor targeting and tumor penetration have been discussed. However, like many other scientific advances that have recently revolutionized, nanomedicines must be further developed to be mature before their full impact can be realized and taken advantage of. The delivery process, which is extremely complicated and governed by numerous factors, must be capable of overcoming a range of barriers presented by the patient's body, particularly those posed by the tumor itself. In the

future, studies must address the challenges to tackle tumor heterogeneity, incorporate immunotherapy in nanomedicines, and conduct clinical studies to validate new strategies in patients.

Acknowledgements
((Acknowledgements, general annotations, funding. Other references to the title/authors can also appear here, such as "Author 1 and Author 2 contributed equally to this work."))

Received: ((will be filled in by the editorial staff))
Revised: ((will be filled in by the editorial staff))
Published online: ((will be filled in by the editorial staff))

References

[1] M. Roser, H. Ritchie, Cancer, https://ourworldindata.org/cancer, accessed: July, 2019. **2019**.

[2] S. M. Sagnella, J. A. McCarroll, M. Kavallaris, *Nanomedicine* **2014**, *10*, 1131-1137.

[3] X. F. Chen, W. J. Zhang, *Chem. Soc. Rev.* **2017**, *46*, 734-760.

[4] R. Chen, J. F. Zhang, Y. Wang, X. F. Chen, J. A. Zapien, C. S. Lee, *Nanoscale* **2015**, *7*, 17299-17305.

[5] J. F. Zhang, Y. N. Li, F. F. An, X. H. Zhang, X. F. Chen, C. S. Lee, *Nano Lett.* **2015**, *15*, 313-318.

[6] L. Yan, W. Chen, X. Y. Zhu, L. B. Huang, Z. G. Wang, G. Y. Zhu, V. A. L. Roy, K. N. Yu, X. F. Chen, *Chem. Commun.* **2013**, *49*, 10938-10940.

[7] F. Xiong, S. X. Huang, N. Gu, *Drug Dev. Ind. Pharm*. **2018**, *44*, 697-706.

[8] C. T. Yu, M. J. Zhou, X. J. Zhang, W. J. Wei, X. F. Chen, X. H. Zhang, *Nanoscale* **2015**, *7*, 5683-5690.

[9] C. Y. Zhao, L. H. Shao, J. Q. Lu, X. W. Deng, Y. J. Tong, Y. Wu, *ACS Appl. Mater. Interfaces* **2017**, *9*, 18450-18461.

[10] X. X. Dai, K. Han, Z. Y. Ma, H. Y. Han, *Adv. Funct. Mater.* **2018**, *28*, 1804609.

[11] Q. W. Zhu, X. J. Chen, X. Xu, Y. Zhang, C. Zhang, R. Mo, *Adv. Funct. Mater.* **2018**, *28*, 1707371.

[12] J. Kolosnjaj-Tabi, R. Di Corato, L. Lartigue, I. Marangon, P. Guardia, A. K. A. Silva, N. Luciani, O. Clement, P. Flaud, J. V. Singh, P. Decuzzi, T. Pellegrino, C. Wilhelm, F. Gazeau, *ACS Nano* **2014**, *8*, 4268-4283.

[13] L. Zhang, H. T. Su, Y. J. Liu, N. Pang, J. Li, X. R. Qi, *J. Controlled Release* **2019,** *294,* 1-16.

[14] A. R. Kirtane, T. Sadhukha, H. Kim, V. Khanna, B. Koniar, J. Panyam, *Cancer Res.* **2017**, *77*, 1465-1475.

[15] D. L. Stirland, J. W. Nichols, E. Jarboe, M. Adelman, M. Dassel, M. M. Janat-Amsbury, Y. H. Bae, *J. Controlled Release* **2015,** *214*, 85-93.

[16] C. H. Heldin, K. Rubin, K. Pietras, A. Ostman, *Nat. Rev. Cancer* **2004**, *4*, 806-813.

[17] T. D. Tailor, G. Hanna, P. S. Yarmolenko, M. R. Dreher, A. S. Betof, A. B. Nixon, I. Spasojevic, M. W. Dewhirst, *Mol. Cancer Ther.* **2010,** *9*, 1798-1808.

[18] A. A. Manzoor, L. H. Lindner, C. D. Landon, J. Y. Park, A. J. Simnick, M. R. Dreher, S. Das, G. Hanna, W. Park, A. Chilkoti, G. A. Koning, T. L. M. ten Hagen, D. Needham, M. W. Dewhirst, *Cancer Res.* **2012,** *72,* 5566-5575.

[19] M. Longmire, P. L. Choyke, H. Kobayashi, *Nanomedicine* **2008**, *3*, 703-717.

[20] K. Xiao, Y. P. Li, J. T. Luo, J. S. Lee, W. W. Xiao, A. M. Gonik, R. G. Agarwal, K. S. Lam, *Biomaterials* **2011**, *32*, 3435-3446.

[21] W. Li, R. C. Luo, X. D. Lin, A. D. Jadhav, Z. C. Zhang, L. Yan, C. Y. Chan, X. F. Chen, J. F. He, C. H. Chen, P. Shi, *Biomaterials* **2015**, *65*, 76-85.

[22] X. Y. Nan, X. J. Zhang, Y. Q. Liu, M. J. Zhou, X. F. Chen, X. H. Zhang, *ACS Appl. Mater. Interfaces* **2017**, *9*, 9986-9995.

[23] A. Senyei, K. Widder, G. Czerlinski, *J. Appl. Phys.* **1978**, *49*, 3578-3583.

[24] R. K. Jain, T. Stylianopoulos, *Nat. Rev. Clin. Oncol.* **2010**, *7*, 653-664.

[25] L. Adamiak, M. A. Touve, C. L. M. LeGuyader, N. C. Gianneschi, *ACS Nano* **2017**, *11*, 9877-9888.

[26] Y. J. Liu, Z. T. Wang, Y. Liu, G. Z. Zhu, O. Jacobson, X. Fu, R. L. Bai, X. Y. Lin, N. Lu, X. Y. Yang, W. P. Fan, J. B. Song, Z. Wang, G. C. Yu, F. W. Zhang, H. Kalish, G. Niu, Z. H. Nie, X. Y. Chen, *ACS Nano* **2017**, *11*, 10539-10548.

[27] G. Prencipe, S. M. Tabakman, K. Welsher, Z. Liu, A. P. Goodwin, L. Zhang, J. Henry, H. J. Dai, *J. Am. Chem. Soc.* **2009**, *131*, 4783-4787.

[28] Z. Liu, C. Davis, W. B. Cai, L. He, X. Y. Chen, H. J. Dai, *Proc. Natl. Acad. Sci. U. S. A.* **2008**, *105*, 1410-1415.

[29] S. Mura, J. Nicolas, P. Couvreur, *Nat. Mater.* **2013**, *12*, 991-1003.

[30] H. Hashizume, P. Baluk, S. Morikawa, J. W. McLean, G. Thurston, S. Roberge, R. K. Jain, D. M. McDonald, *Am. J. Pathol* **2000**, *156*, 1363-1380.

[31] F. Yuan, M. Dellian, D. Fukumura, M. Leunig, D. A. Berk, V. P. Torchilin, R. K. Jain, *Cancer Res.* **1995**, *55*, 3752-3756.

[32] J. W. Nichols, Y. H. Bae, *J. Controlled Release* **2014**, *190*, 451-464.

[33] F. Danhier, *J. Controlled Release* **2016**, *244*, 108-121.

[34] A. Z. Wang, *Sci. Transl. Med.* **2015**, *7*, 294ec112-294ec112.

[35] D. D. Lasic, *Nature* **1996**, *380*, 561-562.

[36] F. M. Muggia, J. D. Hainsworth, S. Jeffers, P. Miller, S. Groshen, M. Tan, L. Roman, B. Uziely, L. Muderspach, A. Garcia, A. Burnett, F. A. Greco, C. P. Morrow, L. J. Paradiso, L. J. Liang, *J. Clin. Oncol.* **1997**, *15*, 987-993.

[37] G. Batist, G. Ramakrishnan, C. S. Rao, A. Chandrasekharan, J. Gutheil, T. Guthrie, P. Shah, A. Khojasteh, M. K. Nair, K. Hoelzer, K. Tkaczuk, Y. C. Park, L. W. Lee, G. Myocet Study, *J. Clin. Oncol.* **2001**, *19*, 1444-1454.

[38] J. Cortes, C. Saura, *EJC Suppl.* **2010**, *8*, 1-10.

[39] V. J. I. p. Kumar Khanna, *ISRN Pharmacol.* **2012**, *2012*, 571394.

[40] Z. L. Cheng, A. Al Zaki, J. Z. Hui, V. R. Muzykantov, A. Tsourkas, *Science* **2012**, *338*, 903-910.

[41] N. Nosrati, R. Abbasi, J. Charmi, A. Rakhshbahar, F. Aliakbarzadeh, H. Danafar, S. Davaran, *Int. J. Biol. Macromol.* **2018**, *117*, 1125-1132.

[42] A. Beck, L. Goetsch, C. Dumontet, N. Corvaia, *Nat. Rev. Drug Discovery* **2017**, *16*, 315-337.

[43] C. Mamot, R. Ritschard, A. Wicki, G. Stehle, T. Dieterle, L. Bubendorf, C. Hilker, S. Deuster, R. Herrmann, C. Rochlitz, *Lancet Oncol.* **2012**, *13*, 1234-1241.

[44] P. A. Ott, R. D. Carvajal, N. Pandit-Taskar, A. A. Jungbluth, E. W. Hoffman, B. W. Wu, J. S. Bomalaski, R. Venhaus, L. D. Pan, L. J. Old, A. C. Pavlick, J. D. Wolchok, *Invest. New Drugs* **2013**, *31*, 425-434.

[45] Q. X. Sun, T. Ojha, F. Kiessling, T. Lammers, Y. Shi, *Biomacromolecules* **2017**, *18*, 1449-1459.

[46] Q. Chen, L. Z. Feng, J. J. Liu, W. W. Zhu, Z. L. Dong, Y. F. Wu, Z. Liu, *Adv. Mater* **2016**, *28*, 7129-7136.

[47] B. Zhang, Y. Hu, Z. Q. Pang, *Front. Pharmacol.* **2017**, *8*, 952.

[48] Z. W. Zhang, H. Wang, T. Tan, J. Li, Z. W. Wang, Y. P. Li, *Adv. Funct. Mater.* **2018**, *28*, 1801840.

[49] A. Orimo, R. A. Weinberg, *Cell Cycle* **2006**, *5*, 1597-1601.

[50] L. E. Roode, H. Brighton, T. Bo, J. L. Perry, M. C. Parrott, F. Kersey, J. C. Luft, J. E. Bear, J. M. DeSimone, I. J. Davis, *Nanomedicine* **2016**, *12*, 1053-1062.

[51] R. V. Iozzo, J. J. Zoeller, A. Nystrom, *Mol. Cells* **2009**, *27*, 503-513.

[52] T. Shen, S. L. Guan, Z. H. Gan, G. Zhang, Q. S. Yu, *Biomacromolecules* **2016**, *17*, 1801-1810.

[53] H. Suzuki, Y. H. Bae, *Biomaterials* **2016**, *98*, 120-130.

[54] F. Chen, K. Ma, B. Madajewski, L. Zhuang, L. Zhang, K. Rickert, M. Marelli, B. Yoo, M. Z. Turker, M. Overholtzer, T. P. Quinn, M. Gonen, P. Zanzonico, A. Tuesca, M. A. Bowen, L. Norton, J. A. Subramony, U. Wiesner, M. S. Bradbury, *Nat. Commun.* **2018**, *9*, 606-606.

[55] F. Y. Liu, X. X. He, H. D. Chen, J. P. Zhang, H. M. Zhang, Z. X. Wang, *Nat. Commun.* **2015**, *6*, 8003.

[56] X. D. Zhang, Z. T. Luo, J. Chen, X. Shen, S. S. Song, Y. M. Sun, S. J. Fan, F. Y. Fan, D. T. Leong, J. P. Xie, *Adv. Mater* **2014**, *26*, 4565-4568.

[57] C. B. He, Y. P. Hu, L. C. Yin, C. Tang, C. H. Yin, *Biomaterials* **2010**, *31*, 3657-3666.

[58] Y. R. Zhang, R. Lin, H. J. Li, W. L. He, J. Z. Du, J. Wang, *Wiley Interdiscip. Rev.: Nanomed. Nanobiotechnol.* **2019**, *11*, e1519.

[59] Y. Kato, S. Ozawa, C. Miyamoto, Y. Maehata, A. Suzuki, T. Maeda, Y. Baba, *Cancer Cell Int.* **2013**, *13*, 89.

[60] P. Swietach, R. D. Vaughan-Jones, A. L. Harris, A. Hulikova, *Philos. Trans. R. Soc., B* **2014**, *369*, 20130099.

[61] L. L. Dai, K. Li, M. H. Li, X. J. Zhao, Z. Luo, L. Lu, Y. F. Luo, K. Y. Cai, *Adv. Funct. Mater.* **2018**, *28*, 1707249.

[62] H. J. Li, J. Z. Du, J. Liu, X. J. Du, S. Shen, Y. H. Zhu, X. Y. Wang, X. D. Ye, S. M. Nie, J. Wang, *ACS Nano* **2016**, *10*, 6753-6761.

[63] J. J. Chen, J. X. Ding, Y. C. Wang, J. J. Cheng, S. X. Ji, X. L. Zhuang, X. S. Chen, *Adv. Mater* **2017**, *29*, 1701170.

[64] A. Jablonska-Trypuc, M. Matejczyk, S. Rosochacki, *J. Enzyme Inhib. Med. Chem.* **2016**, *31*, 177-183.

[65] Y. Liu, D. Zhang, Z. Y. Qiao, G. B. Qi, X. J. Liang, X. G. Chen, H. Wang, *Adv. Mater* **2015**, *27*, 5034–5042.

[66] H. Gerwien, S. Hermann, X. L. Zhang, E. Korpos, J. Song, K. Kopka, A. Faust, C. Wenning, C. C. Gross, L. Honold, N. Melzer, G. Opdenakker, H. Wiendl, M. Schafers, L. Sorokin, *Sci. Transl. Med.* **2016**, *8*, 364ra152.

[67] Y. Q. Lv, C. R. Xu, X. M. Zhao, C. S. Lin, X. Yang, X. F. Xin, L. Zhang, C. Qn, X. P. Han, L. Yang, W. He, L. F. Yin, *ACS Nano* **2018**, *12*, 1519-1536.

[68] C. Wong, T. Stylianopoulos, J. A. Cui, J. Martin, V. P. Chauhan, W. Jiang, Z. Popovic, R. K. Jain, M. G. Bawendi, D. Fukumura, *Proc. Natl. Acad. Sci. U. S. A.* **2011**, *108*, 2426-2431.

[69] S. B. Ruan, X. Cao, X. L. Cun, G. L. Hu, Y. Zhou, Y. J. Zhang, L. B. Lu, Q. He, H. L. Gao, *Biomaterials* **2015**, *60*, 100-110.

[70] Y. Hong, G. H. Nam, E. Koh, S. Jeon, G. B. Kim, C. Jeong, D. H. Kim, Y. Yang, I. S. Kim, *Adv. Funct. Mater.* **2018**, *28*, 1703074.

[71] J. Wang, J. Liu, Y. Liu, L. M. Wang, M. J. Cao, Y. L. Ji, X. C. Wu, Y. Y. Xu, B. Bai, Q. Miao, C. Y. Chen, Y. L. Zhao, *Adv. Mater* **2016**, *28*, 8950-8958.

[72] L. Hua, Z. Wang, L. Zhao, H. L. Mao, G. H. Wang, K. R. Zhang, X. J. Liu, D. M. Wu, Y. L. Zheng, J. Lu, R. T. Yu, H. M. Liu, *Theranostics* **2018**, *8*, 5088-5105.

[73] A. Dirkse, A. Golebiewska, T. Buder, P. V. Nazarov, A. Muller, S. Poovathingal, N. H. Brons, S. Leite, N. Sauvageot, D. Sarkisjan, M. Seyfrid, S. Fritah, D. Stieber, A. Michelucci, F. Hertel, C. Herold-Mende, F. Azuaje, A. Skupin, R. Bjerkvig, A. Deutsch, A. Voss-Bohme, S. P. Niclou, *Nat. Commun.* **2019**, *10*, 1787.

[74] B. Ma, H. C. Cheng, C. L. Mu, G. F. Geng, T. Zhao, Q. Luo, K. L. Ma, R. Chang, Q. Q. Liu, R. Z. Gao, J. L. Nie, J. Y. Xie, J. X. Han, L. B. Chen, G. Ma, Y. S. Zhu, Q. Chen, *Nat. Commun.* **2019**, *10*, 1034.

[75] J. T. Xu, W. Han, P. P. Yang, T. Jia, S. M. Dong, H. T. Bi, A. Gulzar, D. Yang, S. L. Gai, F. He, J. Lin, C. X. Li, *Adv. Funct. Mater.* **2018**, *28*, 1803804.

[76] J. Garcia-Bermudez, L. Baudrier, K. La, X. G. Zhu, J. Fidelin, V. O. Sviderskiy, T. Papagiannakopoulos, H. Molina, M. Snuderl, C. A. Lewis, R. L. Possemato, K. Birsoy, *Nat. Cell Biol.* **2018**, *20*, 775–781.

[77] J. Wojton, Z. T. Chu, H. Mathsyaraja, W. H. Meisen, N. Denton, C. H. Kwon, L. M. L. Chow, M. Palascak, R. Franco, T. Bourdeau, S. Thornton, M. C. Ostrowski, B. Kaur, X. Y. Qi, *Mol. Ther.* **2013**, *21*, 1517-1525.

[78] W. L. Wang, L. Lin, X. J. Ma, B. Wang, S. R. Liu, X. X. Yan, S. R. Li, H. Y. Tian, X. F. Yu, *ACS Appl. Mater. Interfaces* **2018**, *10*, 19398-19407.

[79] D. Zhang, M. Wu, Z. X. Cai, N. S. Liao, K. Ke, H. Z. Liu, M. Li, G. Liu, H. H. Yang, X. L. Liu, J. F. Liu, *Adv. Sci.* **2018**, *5*, 1700648.

[80] T. Thambi, V. G. Deepagan, H. Y. Yoon, H. S. Han, S. H. Kim, S. Son, D. G. Jo, C. H. Ahn, Y. D. Suh, K. Kim, I. C. Kwon, D. S. Lee, J. H. Park, *Biomaterials* **2014**, *35*, 1735-1743.

[81] R. Tong, H. H. Chiang, D. S. Kohane, *Proc. Natl. Acad. Sci. U. S. A.* **2013**, *110*, 19048-19053.

[82] J. You, R. Zhang, C. Y. Xiong, M. Zhong, M. Melancon, S. Gupta, A. M. Nick, A. K. Sood, C. Li, *Cancer Res.* **2012**, *72*, 4777-4786.

[83] X. L. Cun, M. Li, S. Y. Wang, Y. F. Wang, J. L. Wang, Z. Z. Lu, R. X. Yang, X. Tang, Z. R. Zhang, Q. He, *Nanoscale* **2018**, *10*, 9935-9948.

[84] C. Hwang, A. J. Sinskey, H. F. Lodish, *Science* **1992**, *257*, 1496-1502.

[85] Q. Zhang, C. N. Shen, N. Zhao, F. J. Xu, *Adv. Funct. Mater.* **2017**, *27*, 1606229.

[86] X. Sun, J. Zhang, C. Yang, Z. Huang, M. Shi, S. Pan, H. Hu, M. Qiao, D. Chen, X. Zhao, *ACS Appl. Mater. Interfaces* **2019**, *11*, 11865-11875.

[87] M. Y. Wu, Q. S. Meng, Y. Chen, L. X. Zhang, M. L. Li, X. J. Cai, Y. P. Li, P. C. Yu, L. L. Zhang, J. L. Shi, *Adv. Mater* **2016**, *28*, 1963–1969.

[88] L. Hou, X. M. Yang, J. X. Ren, Y. C. Wang, H. J. Zhang, Q. H. Feng, Y. Y. Shi, X. N. Shan, Y. J. Yuan, Z. Z. Zhang, *Int. J. Nanomed.* **2016**, *11*, 607-624.

[89] W. J. Wei, X. J. Zhang, X. F. Chen, M. J. Zhou, R. R. Xu, X. H. Zhang, *Nanoscale* **2016**, *8*, 8118-8125.

[90] F. Y. Zhou, B. Feng, T. T. Wang, D. G. Wang, Q. S. Meng, J. F. Zeng, Z. W. Zhang, S. L. Wang, H. J. Yu, Y. P. Li, *Adv. Funct. Mater.* **2017**, *27*, 1606530.

[91] Y. F. Jiao, Y. F. Sun, B. S. Chang, D. R. Lu, W. L. Yang, *Chem. - Eur. J.* **2013**, *19*, 15410-15420.

[92] V. P. Chauhan, Z. Popovic, O. Chen, J. Cui, D. Fukumura, M. G. Bawendi, R. K. Jain, *Angew. Chem., Int. Ed.* **2011**, *50*, 11417-11420.

[93] S. Dasgupta, T. Auth, G. Gompper, *Nano Lett.* **2014**, *14*, 687-693.

[94] M. J. Zhou, X. J. Zhang, C. T. Yu, X. Y. Nan, X. F. Chen, X. H. Zhang, *Nanomedicine* **2016**, *12*, 181-189.

[95] B. D. Chithrani, A. A. Ghazani, W. C. W. Chan, *Nano Lett.* **2006**, *6*, 662-668.

[96] Z. H. Wang, Y. H. Wang, X. Q. Jia, Q. J. Han, Y. X. Qian, Q. Li, J. F. Xiang, Q. Wang, Z. Y. Hu, W. Z. Wang, *Theranostics* **2019**, *9*, 1728-1740.

[97] C. F. Song, T. T. Lin, Q. Zhang, S. Thayumanavan, L. Ren, *J. Controlled Release* **2019**, *293*, 1-9.

[98] S. Ohta, D. Glancy, W. C. W. Chan, *Science* **2016**, *351*, 841-845.

[99] S. R. Saptarshi, A. Duschl, A. L. Lopata, *J. Nanobiotechnol.* **2013**, *11*, 26.

[100] Q. G. Xu, L. M. Ensign, N. J. Boylan, A. Schon, X. Q. Gong, J. C. Yang, N. W. Lamb, S. T. Cai, T. Yu, E. Freire, J. Hanes, *ACS Nano* **2015**, *9*, 9217-9227.

[101] J. S. Suk, Q. G. Xu, N. Kim, J. Hanes, L. M. Ensign, *Adv. Drug Delivery Rev.* **2016**, *99*, 28-51.

[102] E. A. Sykes, J. Chen, G. Zheng, W. C. W. Chan, *ACS Nano* **2014**, *8*, 5696-5706.

[103] E. Ruoslahti, *Adv. Drug Delivery Rev.* **2017**, *110*, 3-12.

[104] K. Cherukula, W. K. Bae, J. H. Lee, I. K. Park, *Biomaterials* **2018**, *169*, 45-60.

[105] H. Y. Hu, J. Wang, H. Wang, T. Tang, J. Li, Z. W. Wang, K. X. Sun, Y. P. Li, Z. W. Zhang, *Theranostics* **2018**, *8*, 3597-3610.

[106] L. Paasonen, S. Sharma, G. B. Braun, V. R. Kotamraju, T. D. Y. Chung, Z. G. She, K. N. Sugahara, M. Yliperttula, B. A. Wu, M. Pellecchia, E. Ruoslahti, T. Teesalu, *Chembiochem* **2016**, *17*, 570-575.

[107] E. J. Kwon, J. S. Dudani, S. N. Bhatia, *Nat. Biomed. Eng.* **2017**, *1*, 0054.

[108] L. Zhang, Y. Wang, Y. T. Yang, Y. Y. Liu, S. B. Ruan, Q. Y. Zhang, X. W. Tai, J. T. Chen, T. Xia, Y. Qin, H. L. Gao, Q. He, *ACS Appl. Mater. Interfaces* **2015**, *7*, 9691-9701.

[109] Y. P. Zhang, Y. Liu, X. F. Gao, X. M. Li, X. Y. Niu, Z. Yuan, W. Wang, *Acta Biomaterialia* **2019**, *90*, 314-323.

[110] X. Dong, H. J. Liu, H. Y. Feng, S. C. Yang, X. L. Liu, X. Lai, Q. Lu, J. F. Lovell, H. Z. Chen, C. Fang, *Nano Lett.* **2019**, *19*, 997-1008.

[111] H. Gong, Y. Chao, J. Xiang, X. Han, G. S. Song, L. Z. Feng, J. J. Liu, G. B. Yang, Q. Chen, Z. Liu, *Nano Lett.* **2016**, *16*, 2512-2521.

[112] X. X. Han, Y. Y. Li, Y. Xu, X. Zhao, Y. L. Zhang, X. Yang, Y. W. Wang, R. F. Zhao, G. J. Anderson, Y. L. Zhao, G. J. Nie, *Nat. Commun.* **2018**, *9*, 3390.

[113] B. Zhang, T. Jiang, S. Shen, X. J. She, Y. Y. Tuo, Y. Hu, Z. Q. Pang, X. G. Jiang, *Biomaterials* **2016**, *103*, 12-21.

[114] J. Zhang, J. S. Liu, *Pharmacol. Ther.* **2013**, *137*, 200-215.

[115] N. Pang, J. Li, A. N. Sun, Z. Z. Yang, S. X. Cheng, X. R. Qi, *Int. J. Nanomed.* **2018**, *13*, 5971-5990.

[116] H. K. Erickson, P. U. Park, W. C. Widdison, Y. V. Kovtun, L. M. Garrett, K. Hoffman, R. J. Lutz, V. S. Goldmacher, W. A. Blattler, *Cancer Res.* **2006**, *66*, 4426-4433.

[117] Y. Bao, H. H. Guo, Y. L. Lu, W. M. Feng, X. R. Sun, C. W. Tang, X. Wang, M. Shen, *Oncotarget* **2016**, *7*, 77183-77195.

[118] D. D. Sun, Y. N. Liu, Q. Q. Yu, Y. H. Zhou, R. Zhang, X. J. Chen, A. Hong, J. Liu, *Biomaterials* **2013**, *34*, 171-180.

[119] K. C. Valkenburg, A. E. de Groot, K. J. Pienta, *Nat. Rev. Clin. Oncol.* **2018**, *15*, 366-381.

[120] T. J. Ji, Y. P. Ding, Y. Zhao, J. Wang, H. Qin, X. M. Liu, J. Y. Lang, R. F. Zhao, Y. L. Zhang, J. Shi, N. Tao, Z. H. Qin, G. J. Nie, *Adv. Mater* **2015**, *27*, 1865-1873.

[121] J. E. Park, M. C. Lenter, R. N. Zimmermann, P. Garin-Chesa, L. J. Old, W. J. Rettig, *J. Biol. Chem.* **1999**, *274*, 36505-36512.

[122] L. Miao, Y. H. Wang, C. M. Lin, Y. Xiong, N. H. Chen, L. Zhang, W. Y. Kim, L. Huang, *J. Controlled Release* **2015**, *217*, 27-41.

[123] S. Lee, H. Han, H. Koo, J. H. Na, H. Y. Yoon, K. E. Lee, H. Lee, H. Kim, I. C. Kwon, K. Kim, *J. Controlled Release* **2017**, *263*, 68-78.

[124] V. P. Chauhan, T. Stylianopoulos, J. D. Martin, Z. Popovic, O. Chen, W. S. Kamoun, M. G. Bawendi, D. Fukumura, R. K. Jain, *Nat. Nanotechnol.* **2012**, *7*, 383-388.

[125] M. A. Iniguez, A. Rodriguez, O. V. Volpert, M. Fresno, J. M. Redondo, *Trends Mol. Med.* **2003**, *9*, 73-78.

[126] H. S. Kim, A. Sharma, W. X. Ren, J. Y. Han, J. S. Kim, *Biomaterials* **2018**, *185*, 63-72.

[127] B. Zhang, K. Jin, T. Jiang, L. T. Wang, S. Shen, Z. M. Luo, Y. Y. Tuo, X. P. Liu, Y. Hu, Z. Q. Pang, *Sci. Rep.* **2017**, *7,* 10071.

[128] C. Y. Lin, H. C. Tseng, H. R. Shiu, M. F. Wu, C. Y. Chou, W. L. Lin, *Int. J. Nanomed.* **2012**, *7*, 2143-2152.

[129] P. Diagaradjane, A. Shetty, J. C. Wang, A. M. Elliott, J. Schwartz, S. Shentu, H. C. Park, A. Deorukhkar, R. J. Stafford, S. H. Cho, J. W. Tunnell, J. D. Hazle, S. Krishnan, *Nano Lett.* **2008**, *8*, 1492-1500.

[130] S. Kunjachan, A. Detappe, R. Kumar, T. Ireland, L. Cameron, D. E. Biancur, V. Motto-Ros, L. Sancey, S. Sridhar, G. M. Makrigiorgos, R. I. Berbeco, *Nano Lett.* **2015**, *15*, 7488-7496.

[131] A. B. Satterlee, J. D. Rojas, P. A. Dayton, L. Huang, *Theranostics* **2017**, *7*, 253-269.

[132] B. Theek, M. Baues, T. Ojha, D. Mockel, S. K. Veettil, J. Steitz, L. van Bloois, G. Storm, F. Kiessling, T. Lammers, *J. Controlled Release* **2016**, *231*, 77-85.

[133] R. J. Akhurst, A. Hata, *Nat. Rev. Drug Discovery* **2012**, *11*, 790-811.

[134] C. Margadant, A. Sonnenberg, *EMBO Rep.* **2010**, *11*, 97-105.

[135] H. Cabral, Y. Matsumoto, K. Mizuno, Q. Chen, M. Murakami, M. Kimura, Y. Terada, M. R. Kano, K. Miyazono, M. Uesaka, N. Nishiyama, K. Kataoka, *Nat. Nanotechnol.* **2011**, *6*, 815-823.

[136] G. Yang, S. Z. F. Phua, W. Q. Lim, R. Zhang, L. Feng, G. Liu, H. Wu, A. K. Bindra, D. Jana, Z. Liu, Y. Zhao, *Adv. Mater* **2019**, *31*, 1901513.

[137] F. Gong, L. Cheng, N. Yang, O. Betzer, L. Feng, Q. Zhou, Y. Li, R. Chen, R. Popovtzer, Z. Liu, *Adv. Mater* **2019**, *31*, 1900730.

[138] Q. Chen, L. G. Xu, J. W. Chen, Z. J. Yang, C. Liang, Y. Yang, Z. Liu, *Biomaterials* **2017**, *148*, 69-80.

[139] P. Vaupel, L. Harrison, *Oncologist* **2004**, *9*, 4-9.

[140] D. L. Xia, P. P. Xu, X. Y. Luo, J. F. Zhu, H. Y. Gu, D. Huo, Y. Hu, *Adv. Funct. Mater.* **2019**, *29*, 1807294.

[141] X. J. Song, L. Z. Feng, C. Liang, M. Gao, G. S. Song, Z. Liu, *Nano Research* **2017**, *10*, 1200-1212.

[142] M. Benej, X. Q. Hong, S. Vibhute, S. Scott, J. H. Wu, E. Graves, Q. T. Le, A. C. Koong, A. J. Giaccia, B. Yu, S. C. Chen, I. Papandreou, N. C. Denko, *Proc. Natl. Acad. Sci. U. S. A.* **2018**, *115*, 10756-10761.

[143] E. Milotti, S. Stella, R. Chignola, *Sci. Rep.* **2017**, *7*, 39762.

[144] J. F. Lin, J. Li, A. Gopal, T. Munshi, Y. W. Chu, J. X. Wang, T. T. Liu, B. Y. Shi, X. F. Chen, L. Yan, *Chem. Commun.* **2019**, *55*, 2656-2659.

[145] L. Yan, Z. G. Wang, X. F. Chen, X. J. Gou, Z. Y. Zhang, X. Y. Zhu, M. H. Lan, W. Chen, G. Y. Zhu, W. J. Zhang, *Chem. Commun.* **2017**, *53*, 2339-2342.

[146] D. Min, D. Jeong, M. G. Choi, K. Na, *Biomaterials* **2015**, *52*, 484-493.

[147] C. G. Qian, J. C. Yu, Y. L. Chen, Q. Y. Hu, X. Z. Xiao, W. J. Sun, C. Wang, P. J. Feng, Q. D. Shen, Z. Gu, *Adv. Mater* **2016**, *28*, 3313-3320.

[148] X. L. Huang, J. Chisholm, J. Zhuang, Y. Y. Xiao, G. Duncan, X. Y. Chen, J. S. Suk, J. Hanes, *Proc. Natl. Acad. Sci. U. S. A.* **2017**, *114*, E6595-E6602.

[149] X. L. Huang, J. Zhuang, S. W. Chung, B. W. Huang, G. Halpert, K. Negron, X. R. Sun, J. Yang, Y. Oh, P. M. Hwang, J. Hanes, J. S. Suk, *ACS Nano* **2019**, *13*, 236-247.

[150] Y. Kim, Q. Lin, P. M. Glazer, Z. Yun, *Curr. Mol. Med.* **2009**, *9*, 425-434.

[151] T. Y. Wang, K. E. Wilson, S. Machtaler, J. K. Willmann, *Curr. Pharm. Biotechnol.* **2013**, *14*, 743-752.

[152] A. M. Malekzadeh, A. Ramazani, S. J. T. Rezaei, H. Niknejad, *J. Colloid Interface Sci.* **2017**, *490*, 64-73.

[153] A. Nacev, A. Komaee, A. Sarwar, R. Probst, S. H. Kim, M. Emmert-Buck, B. Shapiro, *IEEE Control Syst. Mag.* **2012**, *32*, 32-74.

[154] A. S. Lubbe, C. Bergemann, H. Riess, F. Schriever, P. Reichardt, K. Possinger, M. Matthias, B. Dorken, F. Herrmann, R. Gurtler, P. Hohenberger, N. Haas, R. Sohr, B. Sander, A. J. Lemke, D. Ohlendorf, W. Huhnt, D. Huhn, *Cancer Res.* **1996**, *56*, 4686-4693.

[155] O. Felfoul, M. Mohammadi, S. Taherkhani, D. de Lanauze, Y. Z. Xu, D. Loghin, S. Essa, S. Jancik, D. Houle, M. Lafleur, L. Gaboury, M. Tabrizian, N. Kaou, M. Atkin, T. Vuong, G. Batist, N. Beauchemin, D. Radzioch, S. Martel, *Nat. Nanotechnol.* **2016**, *11*, 941-947.

[156] X. M. Guo, Z. Wu, W. Li, Z. H. Wang, Q. P. Li, F. F. Kong, H. B. Zhang, X. L. Zhu, Y. P. P. Du, Y. Jin, Y. Z. Du, J. You, *ACS Appl. Mater. Interfaces* **2016**, *8*, 3092-3106.

[157] M. Shamsi, A. Sedaghatkish, M. Dejam, M. Saghafian, M. Mohammadi, A. Sanati-Nezhad, *Drug Delivery* **2018**, *25*, 846-861.

[158] M. Muthana, A. J. Kennerley, R. Hughes, E. Fagnano, J. Richardson, M. Paul, C. Murdoch, F. Wright, C. Payne, M. F. Lythgoe, N. Farrow, J. Dobson, J. Conner, J. M. Wild, C. Lewis, *Nat. Commun.* **2015**, *6,* 8009.

[159] S. Schuerle, A. P. Soleimany, T. Yeh, G. M. Anand, M. Häberli, H. E. Fleming, N. Mirkhani, F. Qiu, S. Hauert, X. Wang, B. J. Nelson, S. N. Bhatia, *Sci. Adv.* **2019**, *5*, eaav4803.

[160] P. Lam, R. D. Lin, N. F. Steinmetz, *J. Mater. Chem. B* **2018**, *6*, 5888-5895.

[161] T. D. McKee, P. Grandi, W. Mok, G. Alexandrakis, N. Insin, J. P. Zimmer, M. G. Bawendi, Y. Boucher, X. O. Breakefield, R. K. Jain, *Cancer Res.* **2006**, *66*, 2509-2513.

[162] A. E. Smith, A. Helenius, *Science* **2004**, *304*, 237-242.

[163] H. B. Xia, Q. W. Mao, B. L. Davidson, *Nat. Biotechnol.* **2001**, *19*, 640-644.

[164] S. Kilcher, J. Mercer, *Virology* **2015**, *479*, 578-590.

[165] B. Huang, D. J. Irvine, *Cancer Res.* **2011**, *71*, 4432-4432.

[166] M. Bernardes-Silva, D. C. Anthony, A. C. Issekutz, V. H. Perry, *J. Cereb. Blood Flow Metab.* **2001**, *21*, 1115-1124.

[167] J. W. Xue, Z. K. Zhao, L. Zhang, L. J. Xue, S. Y. Shen, Y. J. Wen, Z. Y. Wei, L. Wang, L. Y. Kong, H. B. Sun, Q. N. Ping, R. Mo, C. Zhang, *Nat. Nanotechnol.* **2017**, *12*, 692-700.

[168] X. Zhang, X. H. Xu, Y. C. Li, C. Hu, Z. J. Zhang, Z. W. Gu, *Adv. Mater* **2018**, *30*, 1707240.

[169] Y. Takechi-Haraya, Y. Goda, K. Sakai-Kato, *Mol. Pharmaceutics* **2017**, *14*, 2158-2165.

[170] L. Zhang, P. Y. Hao, D. J. Yang, S. Feng, B. Peng, D. Appelhans, T. H. Zhang, X. J. Zan, *J. Mater. Chem. B* **2019**, *7*, 953-964.

[171] F. Peng, M. I. Setyawati, J. K. Tee, X. G. Ding, J. P. Wang, M. E. Nga, H. K. Ho, D. T. Leong, *Nat. Nanotechnol.* **2019**, *14*, 279–286.

[172] X. F. Chen, *Adv. Drug Delivery Rew.* **2018**, *127*, 85-105.

[173] N. N. Zhao, L. M. Yan, X. Y. Zhao, X. Y. Chen, A. H. Li, D. Zheng, X. Zhou, X. G. Dai, F. J. Xu, *Chem. Rev.* **2019**, *119*, 1666-1762.

[174] R. R. Wang, Y. Hu, N. N. Zhao, F. J. Xu, *ACS Appl. Mater. Interfaces* **2016**, *8*, 11298-11308.

[175] S. Duan, Y. J. Yang, C. L. Zhang, N. N. Zhao, F. J. Xu, *Small* **2017**, *13,* 1603133.

[176] Y. X. Qian, Y. H. Wang, F. Jia, Z. H. Wang, C. Y. Yue, W. K. Zhang, Z. Y. Hu, W. Z. Wang, *Biomaterials* **2019**, *188*, 96-106.

[177] T. T. Wang, D. G. Wang, J. P. Liu, B. Feng, F. Y. Zhou, H. W. Zhang, L. Zhou, Q. Yin, Z. W. Zhang, Z. L. Cao, H. J. Yu, Y. P. Li, *Nano Lett.* **2017**, *17*, 5429-5436.

[178] R. Agarwal, P. Jurney, M. Raythatha, V. Singh, S. V. Sreenivasan, L. Shi, K. Roy, *Adv. Healthcare Mater.* **2015**, *4*, 2269-2280.

[179] K. P. Valente, S. S. Thind, M. Akbari, A. Suleman, A. G. Brolo, *ACS Biomater. Sci. Eng.* **2019**, *5*, 2887-2898.

[180] A. Albanese, A. K. Lam, E. A. Sykes, J. V. Rocheleau, W. C. W. Chan, *Nat. Commun.* **2013**, *4,* 2718.

[181] A. Tchoryk, V. Taresco, R. H. Argent, M. Ashford, P. R. Gellert, S. Stolnik, A. Grabowska, M. C. Garnett, *Bioconjugate Chem.* **2019**, *30*, 1371-1384.

[182] J. Friedrich, C. Seidel, R. Ebner, L. A. Kunz-Schughart, *Nat. Protoc.* **2009**, *4*, 309-324.

[183] M. R. DeWitt, M. N. Rylander, in *Targeted Drug Delivery: Methods and Protocols,* Vol. 1831 (Eds: R. W. Sirianni, B. Behkam), **2018**, pp. 159-178.

[184] N. E. Clay, K. Shin, A. Ozcelildalei, M. K. Lee, M. H. Rich, D. H. Kim, B. Han, H. Kong, *ACS Biomater. Sci. Eng.* **2016**, *2*, 1968-1975.

[185] H. Jin, T. Zhu, X. G. Huang, M. Sun, H. G. Li, X. Y. Zhu, M. L. Liu, Y. B. Xie, W. Huang, D. Y. Yan, *Biomaterials* **2019**, *211*, 68-80.

[186] C. Wang, S. Q. Chen, Y. X. Wang, X. R. Liu, F. Q. Hu, J. H. Sun, H. Yuan, *Adv. Mater* **2018**, *30*, 1706407.

[187] C. Y. Ju, R. Mo, J. W. Xue, L. Zhang, Z. K. Zhao, L. J. Xue, Q. N. Ping, C. Zhang, *Angew. Chem., Int. Ed.* **2014**, *53*, 6253-6258.

[188] C. Denkert, S. Loibl, A. Noske, M. Roller, B. M. Muller, M. Komor, J. Budczies, S. Darb-Esfahani, R. Kronenwett, C. Hanusch, C. von Torne, W. Weichert, K. Engels, C. Solbach, I. Schrader, M. Dietel, G. von Minckwitz, *J. Clin. Oncol.* **2010**, *28*, 105-113.

[189] D. V. Krysko, A. D. Garg, A. Kaczmarek, O. Krysko, P. Agostinis, P. Vandenabeele, *Nat. Rev. Cancer* **2012**, *12*, 860-875.

[190] K. E. de Visser, A. Eichten, L. M. Coussens, *Nat. Rev. Cancer* **2006**, *6*, 24-37.

[191] S. I. Grivennikov, F. R. Greten, M. Karin, *Cell* **2010**, *140*, 883-899.

[192] E. Lanitis, D. Dangaj, M. Irving, G. Coukos, *Annals of Oncolol.* **2017**, *28*, 18-32.

[193] M. P. Vadevoo, S. Gurung, F. Khan, M. E. Haque, G. R. Gunassekaran, L. H. Chi, U. Permpoon, B. Lee, *Arch. Pharmacal Res.* **2019**, *42*, 150-158.

[194] Y. Z. Chen, W. T. Song, L. M. Shen, N. S. Qiu, M. Y. Hu, Y. Liu, Q. Liu, L. Huang, *ACS Nano* **2019**, *13*, 1751-1763.

[195] X. W. Guan, L. Lin, J. Chen, Y. Y. Hu, P. J. Sun, H. Y. Tian, A. Maruyama, X. S. Chen, *J. Controlled Release* **2019**, *293*, 104-112.

[196] M. E. Davis, *Mol. Pharmaceutics* **2009**, *6*, 659-668.

[197] A. Wicki, D. Witzigmann, V. Balasubramanian, J. Huwyler, *J. Controlled Release* **2015**, *200*, 138-157.

[198] Y. X. Tang, Y. H. Li, S. Li, H. Hu, Y. X. Wu, C. Xiao, Z. Q. Chu, Z. F. Li, X. L. Yang, *Nanoscale* **2019**, *11*, 6217-6227.

[199] H. J. Li, J. Z. Du, X. J. Du, C. F. Xu, C. Y. Sun, H. X. Wang, Z. T. Cao, X. Z. Yang, Y. H. Zhu, S. M. Nie, J. Wang, *Proc. Natl. Acad. Sci. U. S. A.* **2016**, *113*, 4164-4169.

[200] Z. Popovic, W. H. Liu, V. P. Chauhan, J. Lee, C. Wong, A. B. Greytak, N. Insin, D. G. Nocera, D. Fukumura, R. K. Jain, M. G. Bawendi, *Angew. Chem., Int. Ed.* **2010**, *49*, 8649-8652.

[201] E. A. Nance, G. F. Woodworth, K. A. Sailor, T. Y. Shih, Q. G. Xu, G. Swaminathan, D. Xiang, C. Eberhart, J. Hanes, *Sci. Transl. Med.* **2012**, *4*, 149ra119.

[202] H. Lee, H. Fonge, B. Hoang, R. M. Reilly, C. Allen, *Mol. Pharmaceutics* **2010**, *7*, 1195-1208.

[203] T. Wei, J. Liu, H. L. Ma, Q. Cheng, Y. Y. Huang, J. Zhao, S. D. Huo, X. D. Xue, Z. C. Liang, X. J. Liang, *Nano Lett.* **2013**, *13*, 2528-2534.

[204] R. M. Davis, B. Kiss, D. R. Trivedi, T. J. Metzner, J. C. Liao, S. S. Gambhir, *ACS Nano* **2018**, *12*, 9669-9679.

[205] Y. Cong, L. Ji, Y. J. Gao, F. H. Liu, D. B. Cheng, Z. Y. Hu, Z. Y. Qiao, H. Wang, *Angew. Chem., Int. Ed.* **2019**, *58*, 4632-4637.

[206] L. Li, T. L. M. ten Hagen, M. Bolkestein, A. Gasselhuber, J. Yatvin, G. C. van Rhoon, A. M. M. Eggermont, D. Haemmerich, G. A. Koning, *J. Controlled Release* **2013**, *167*, 130-137.

[207] C. Carlier, B. Laforce, S. J. M. Van Malderen, F. Gremonprez, R. Tucoulou, J. Villanova, O. De Wever, L. Vincze, F. Vanhaecke, W. Ceelen, *J. Pharm. Biomed. Anal.* **2016**, *131*, 256-262.

[208] W. C. Huang, W. H. Chiang, Y. H. Cheng, W. C. Lin, C. F. Yu, C. Y. Yen, C. K. Yeh, C. S. Chern, C. S. Chiang, H. C. Chiu, *Biomaterials* **2015**, *71*, 71-83.

[209] Q. Zhou, S. Shao, J. Wang, C. Xu, J. Xiang, Y. Piao, Z. Zhou, Q. Yu, J. Tang, X. Liu, Z. Gan, R. Mo, Z. Gu, Y. Shen, *Nat. Nanotechnol.* **2019,** *10*, 1038.

[210] G. Kroemer, L. Galluzzi, O. Kepp, L. Zitvogel, in *Annual Review of Immunology,* Vol. 31 (Eds: D. R. Littman, W. M. Yokoyama), **2013**, pp. 51-72.

[211] X. D. Xue, Y. Huang, R. N. Bo, B. Jia, H. Wu, Y. Yuan, Z. L. Wang, Z. Ma, D. Jing, X. B. Xu, W. M. Yu, T. Y. Lin, Y. P. Li, *Nat. Commun.* **2018**, *9*, 3653.

[212] S. Tang, Q. S. Meng, H. P. Sun, J. H. Su, Q. Yin, Z. W. Zhang, H. J. Yu, L. L. Chen, W. W. Gu, Y. P. Li, *Biomaterials* **2017**, *114*, 44-53.

[213] C. Hu, X. L. Cun, S. B. Ruan, R. Liu, W. Xiao, X. T. Yang, Y. Y. Yang, C. Y. Yang, H. L. Gao, *Biomaterials* **2018**, *168*, 64-75.

[214] S. Khatoon, H. S. Han, J. Jeon, N. V. Rao, D. W. Jeong, M. Ikram, T. Yasin, G. R. Yi, J. H. Park, *Polymers* **2018**, *10*, 390.

[215] Z. B. Li, M. Wu, H. Z. Bai, X. G. Liu, G. P. Tang, *Chem. Commun.* **2018**, *54*, 13127-13130.

[216] W. D. Ke, W. Yin, Z. S. Zha, J. F. Mukerabigwi, W. J. Chen, Y. H. Wang, C. X. He, Z. S. Ge, *Biomaterials* **2018**, *154*, 261-274.

[217] P. H. Zhang, Y. Wang, J. Lian, Q. Shen, C. Wang, B. H. Ma, Y. C. Zhang, T. T. Xu, J. X. Li, Y. P. Shao, F. Xu, J. J. Zhu, *Adv. Mater* **2017**, *29*, 1702311.

[218] Z. R. Wang, Q. He, W. G. Zhao, J. W. Luo, W. P. Gao, *J. Controlled Release* **2017**, *264*, 66-75.

[219] T. Y. Yong, J. Hu, X. Q. Zhang, F. Y. Li, H. Yang, L. Gan, X. L. Yang, *ACS Appl. Mater. Interfaces* **2016**, *8*, 27611-27621.

[220] Y. J. Zhang, W. Z. Chen, C. C. Yang, Q. L. Fan, W. Wu, X. Q. Jiang, *J. Controlled Release* **2016**, *237*, 115-124.

[221] C. Hu, X. T. Yang, R. Liu, S. B. Ruan, Y. Zhou, W. Xiao, W. Q. Yu, C. Y. Yang, H. L. Gao, *ACS Appl. Mater. Interfaces* **2018**, *10*, 22571-22579.

[222] Y. Jiang, X. Pang, R. L. Liu, Q. C. Xiao, P. Wang, A. W. Leung, Y. X. Luan, C. S. Xu, *ACS Appl. Mater. Interfaces* **2018**, *10*, 31674-31685.

[223] J. E. Zhou, J. Yu, L. P. Gao, L. Sun, T. Peng, J. Wang, J. Z. Zhu, W. Y. Lu, L. Zhang, Z. Q. Yan, L. Yu, *Mol. Pharmaceutics* **2017**, *14*, 1811-1820.

[224] Y. Q. Zhu, Z. Jian, F. H. Meng, D. Chao, C. Ru, J. Feijen, Z. Y. Zhong, *ACS Appl. Mater. Interfaces* **2017**, *9*, 35651-35663.

[225] R. Loria, C. Giliberti, A. Bedini, R. Palomba, G. Caracciolo, P. Ceci, E. Falvo, R. Marconi, R. Falcioni, G. Bossi, L. Strigari, *J. Exp. Clin. Cancer Res.* **2019**, *38*, 11.

[226] W. Feng, R. Wang, Y. Zhou, L. Ding, X. Gao, B. Zhou, P. Hu, Y. Chen, *Adv. Funct. Mater.* **2019**, *29*, 1901942.

[227] J. Kolosnjaj-Tabi, I. Marangon, A. Nicolas-Boluda, A. K. A. Silva, F. Gazeau, *Pharmacol. Res.* **2017**, *126*, 123-137.

[228] L. Beola, L. Asin, R. M. Fratila, V. Herrero, J. M. de la Fuente, V. Grazu, L. Gutierrez, *ACS Appl. Mater. Interfaces* **2018**, *10*, 44301-44313.

[229] N. Schleich, C. Po, D. Jacobs, B. Ucakar, B. Gallez, F. Danhier, V. Preat, *J. Controlled Release* **2014**, *194*, 82-91.

[230] M. Wang, J. J. Li, X. J. Li, H. J. Mu, X. M. Zhang, Y. N. Shi, Y. C. Chu, A. P. Wang, Z. M. Wu, K. X. Sun, *J. Controlled Release* **2016**, *232*, 161-174.

[231] Q. X. Ma, L. Cheng, F. Gong, Z. L. Dong, C. Liang, M. Y. Wang, L. Z. Feng, Y. G. Li, Z. Liu, C. Li, L. He, *J. Mater. Chem. B* **2018**, *6*, 5069-5079.

[232] G. B. Yang, L. G. Xu, Y. Chao, J. Xu, X. Q. Sun, Y. F. Wu, R. Peng, Z. Liu, *Nat. Commun.* **2017**, *8*, 902.

[233] L. Zhang, H. J. Yi, J. Song, J. Huang, K. Yang, B. Tan, D. Wang, N. L. Yang, Z. G. Wang, X. S. Li, *ACS Appl. Mater. Interfaces* **2019**, *11*, 9355-9366.

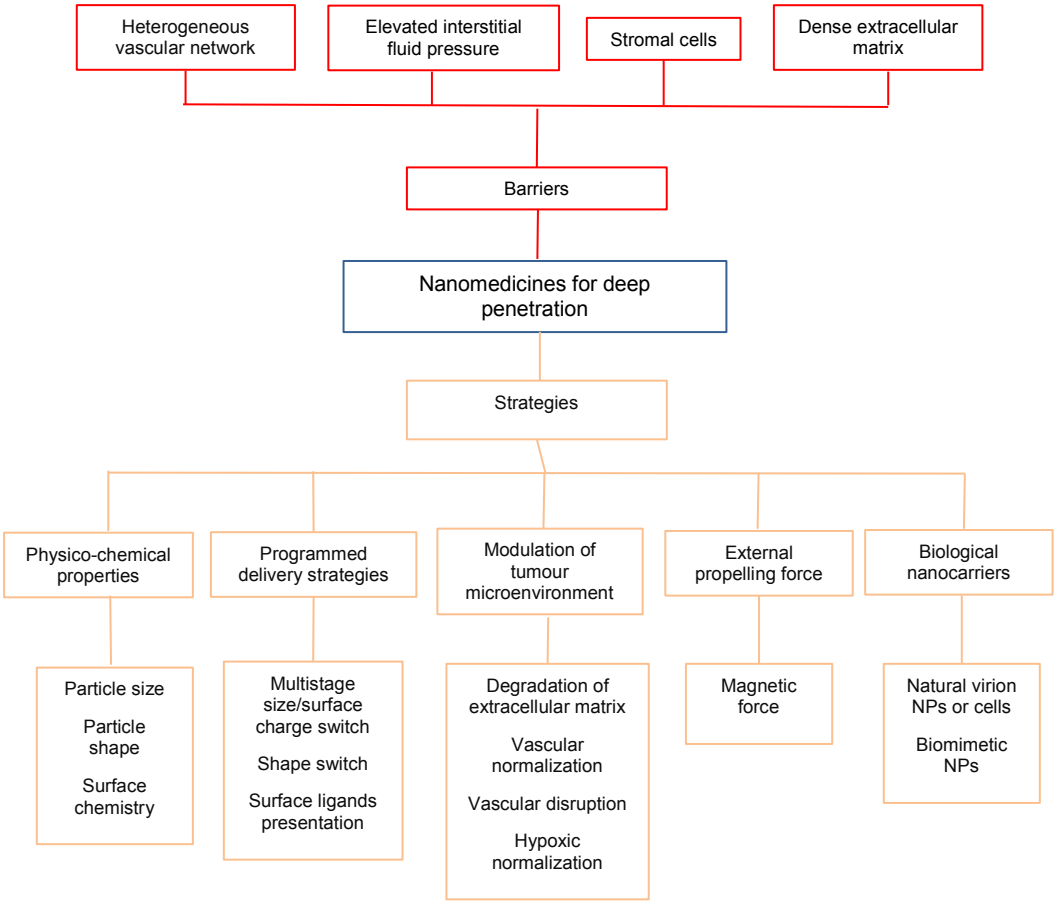

Figure 1. Barriers and strategies to nanomedicines for deep tumor penetration for efficient cancer treatment.

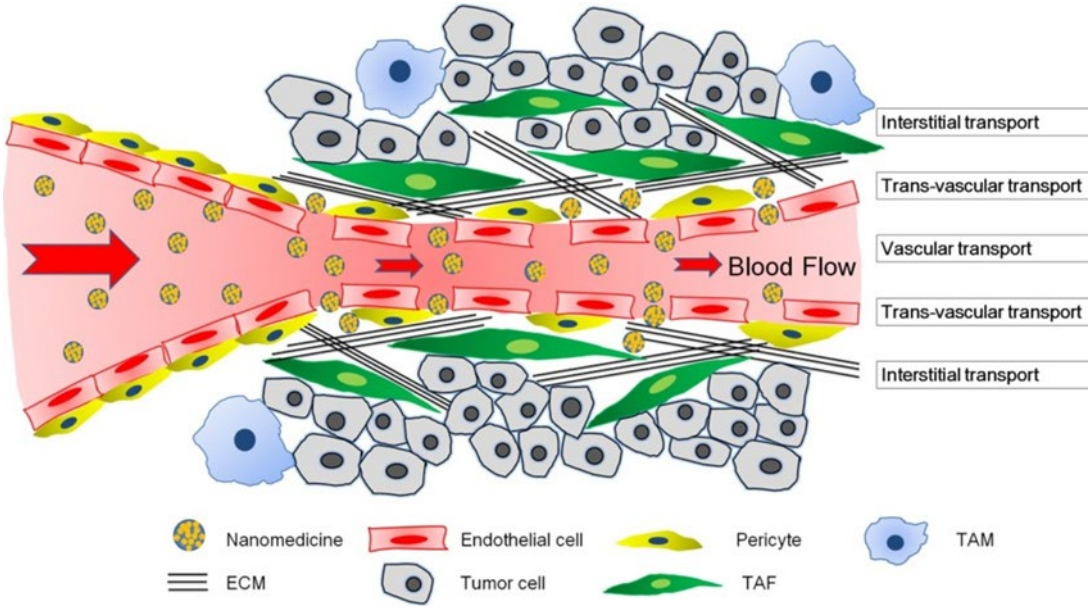

Figure 2. The three transport steps of nanomedicines targeting delivery; Passive targeting (EPR effect) through drug accumulation in leaky vasculature areas. There are no ruptures in the normal tissue, therefore, the drug is transported through the blood vessel steadily. The drug percolates through holes in the tumor-affected region and accumulates within the tumor; The barriers to deep penetration of NPs inflicted by the tumor microenvironment, including IFP, stromal cells and a dense ECM. Reproduced with permission.[47] Copyright 2017, Frontiers in Pharmacology.

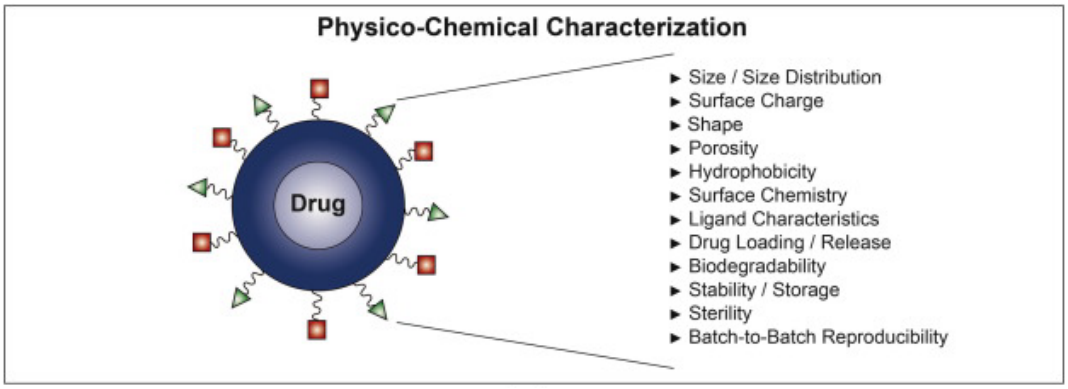

Figure 3. Physico-chemical characterization of a drug. Reproduced with permission.[197] Copyright 2015, Journal of Controlled Release.

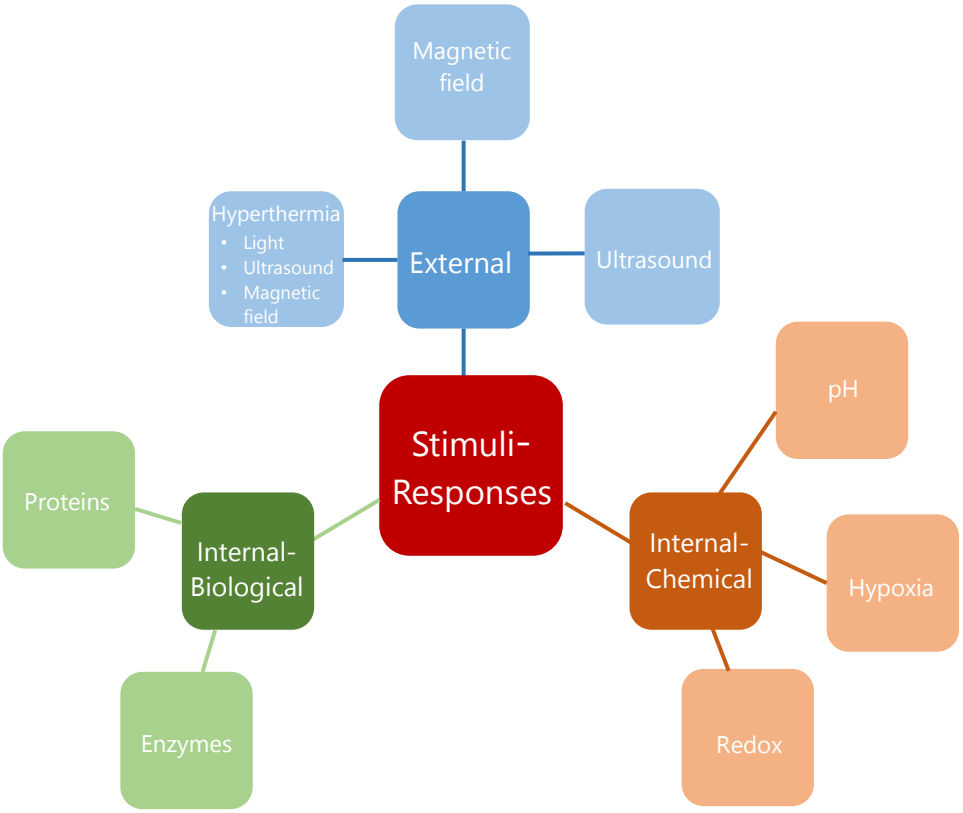

Figure 4. Diagram indicating the main triggers currently being researched for multistage NPs.

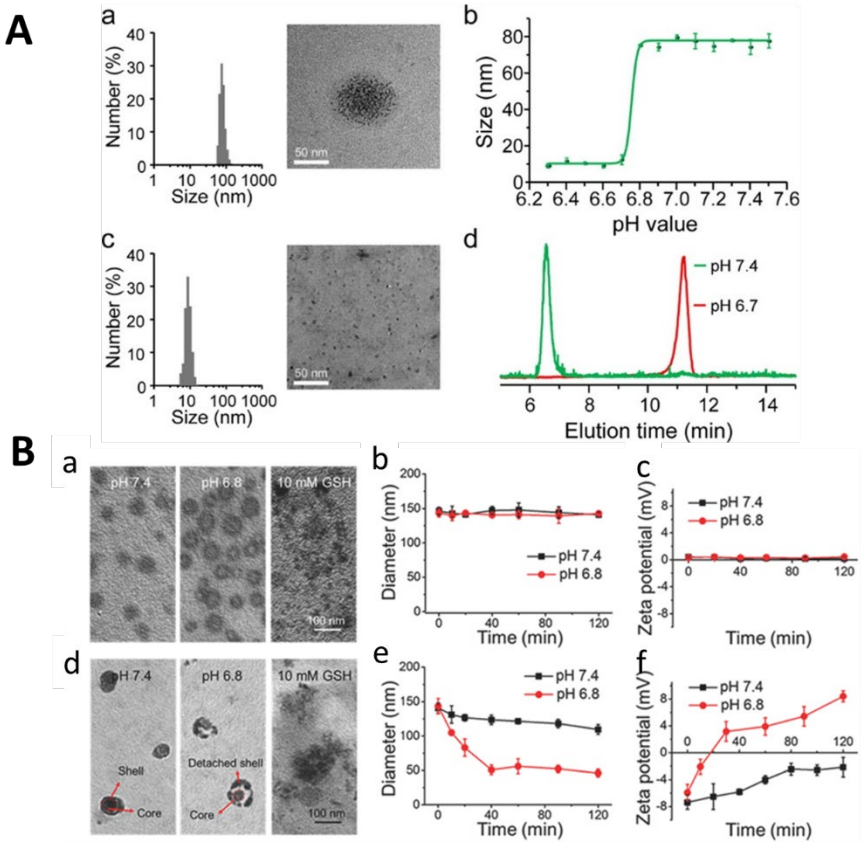

Figure 5. (A) Tumor-pH-triggered size transition of SCNs/Pt. (a) DLS (left panel) and TEM (right panel) measurements of SCNs/Pt in phosphate buffer (PB) at pH 7.4. (b) pH-Dependent size change of SCNs/Pt analyzed by DLS. (c) DLS (left panel) and TEM (right panel) measurements of SCNs/Pt at pH 6.7. (d) Gel filtration chromatography analysis of SCNs/Pt treated at pH 6.7 and 7.4. (B) Self-Assembly and sequential stimuli-responsibilities of SNP. (a,d) Morphologies of a) NP and d) SNP in PBS at pH 7.4 or 6.8 without or with 10.0 mM glutathione (GSH) detected by TEM. (b,e) Changes of zeta potentials of b) NP and e) SNP in PBS at pH 7.4 or 6.8. (c,f) DOX release behaviors of c) NP and f) SNP in PBS at pH 7.4 or 6.8 without or with 10.0 mM GSH. Reproduced with permission.[62-63] Copyright 2016, ACS Nano. Copyright 2017, Advanced Materials.

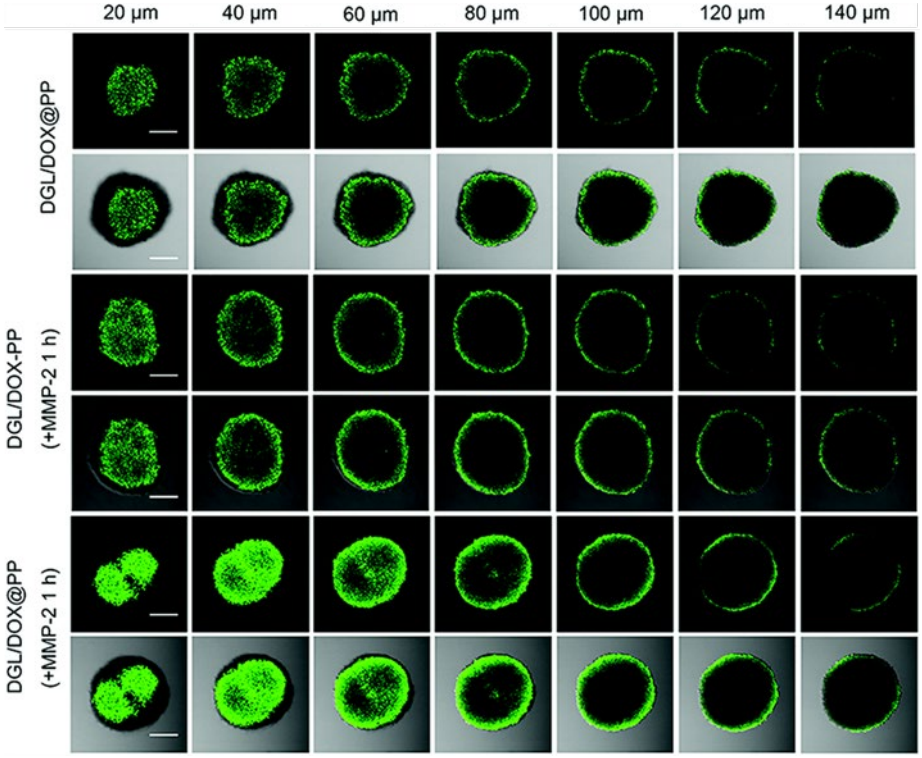

Figure 6. In vitro multicellular tumor spheroid penetration of DGL/DOX@PP, DGL/DOX-PP + MMP-2 1 h (pretreated with 300 ng mL^{-1} MMP-2 for 1 h) and DGL/DOX@PP + MMP-2 1 h (pretreated with 300 ng mL^{-1} MMP-2 for 1 h) after 24 h of incubation in different depths. The concentration of DOX used was 10 μg mL^{-1}. Green represents DOX. Bar represents 200 μm. Reproduced with permission.[83] Copyright 2018, Nanoscale.

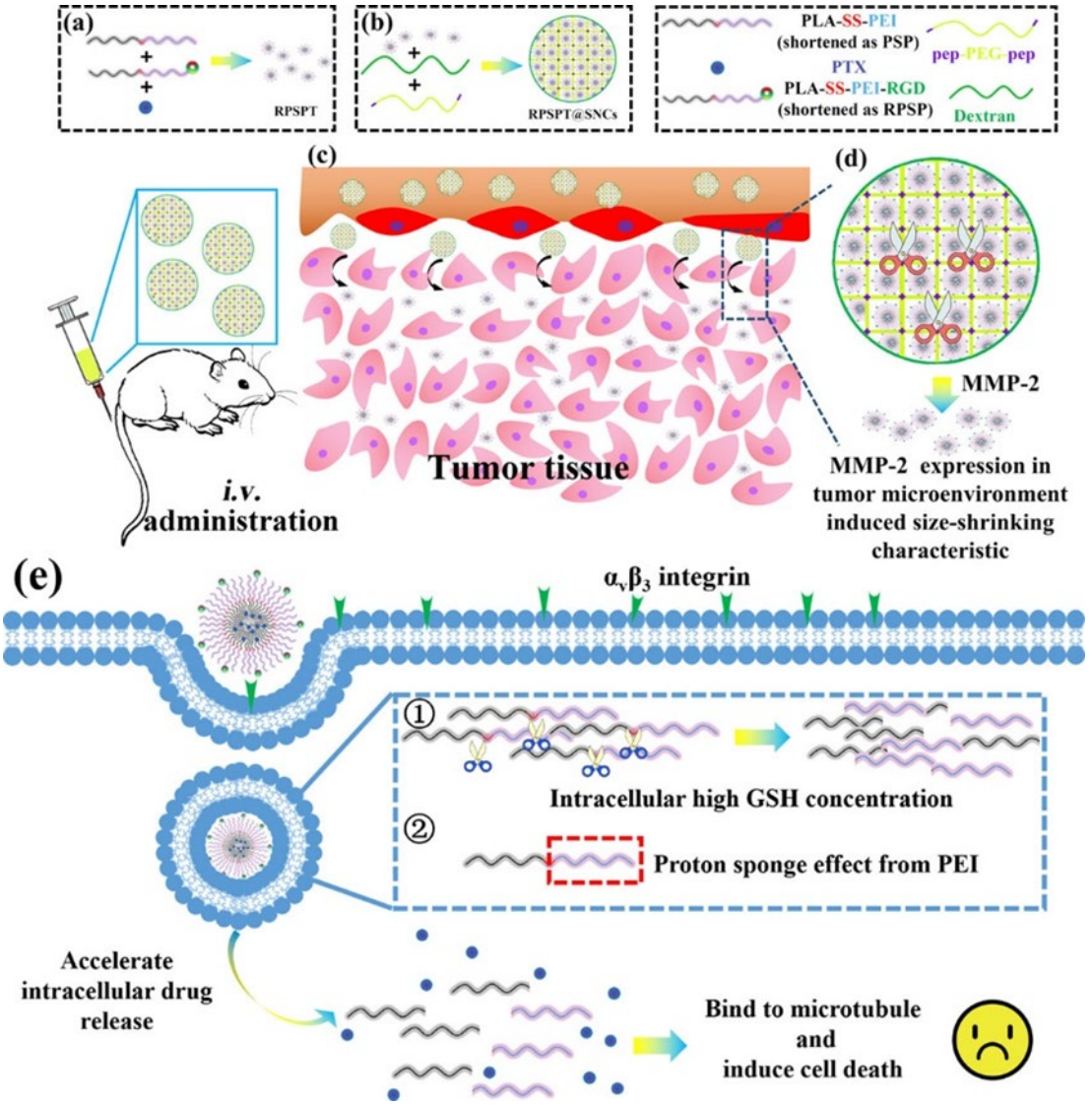

Figure 7. Schematic illustration of hierarchical disassembly of RPSPT@SNCs. A typical RPSPT@SNCs was composed of RGD-mediated, redox-responsive micelles loaded with PTX, which was incorporated into an extracellular matrix metalloproteinase-2-responsive cross-linked network. (a) Preparation procedure of RPSPT. (b) Preparation procedure of RPSPT@SNCs. (c) RPSPT@SNCs could accumulate into tumor tissue via an EPR effect. (d) RPSPT@SNCs could be degraded in the presence of high concentration of MMP-2 and release small-sized RPSPT to possess higher tumor penetration. (e) When RPSPT was accumulated into tumor tissue, it could be internalized into tumor cells via RGD-mediated cell endocytosis. In an acidic endo/lysosomal environment, PEI could possess a proton sponge effect and facilitate endo/lysosome escape. Meanwhile, the disulfide bond would leak in the

presence of high concentration of GSH and eventually lead to intracellular drug accumulation to exert preferable antitumor activity. Reproduced with permission.[86] Copyright 2019, ACS Applied Materials & Interfaces.

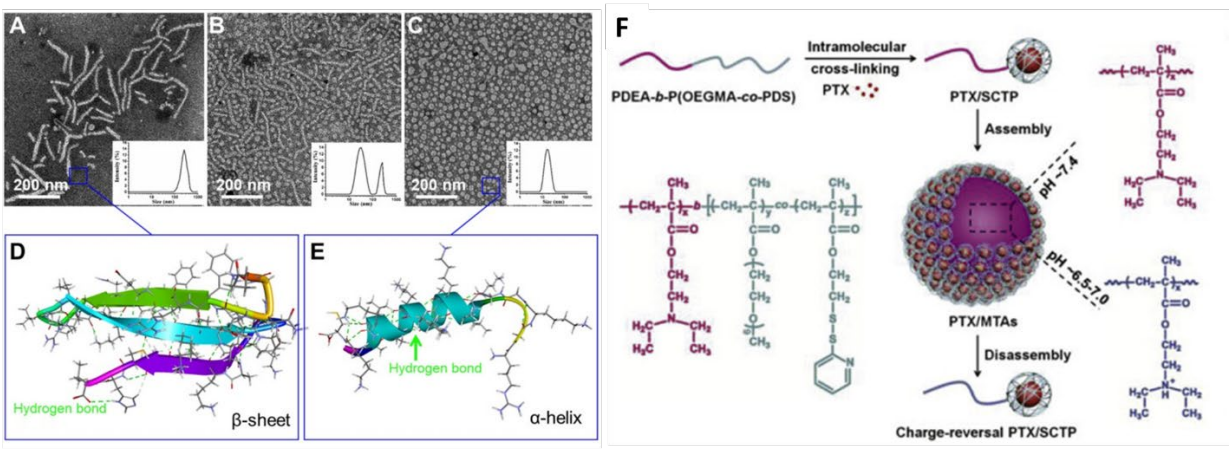

Figure 8. Characterizations of HEKMs. (A) DLS and TEM images of HEKMs without MMP-2. (B) DLS and TEM images of HEKMs incubated with MMP-2 for 2 h. (C) DLS and TEM images of HEKMs incubated with MMP-2 for 4 h. The scale bar indicates 200 nm. (D) Molecular simulation of the secondary structures of HEKMs before MMP-2 cleavage. (E) Molecular simulation of the secondary structures of HEKMs after cleavage. (F) Illustration of the preparation of PTX/MTAs from PDEA-b-P(OEGMA-co-PDS) copolymer and the pH-sensitive morphological transition. Reproduced with permission.[96-97] Copyright 2019, Theranostics. Copyright 2019, Journal of Controlled Release.

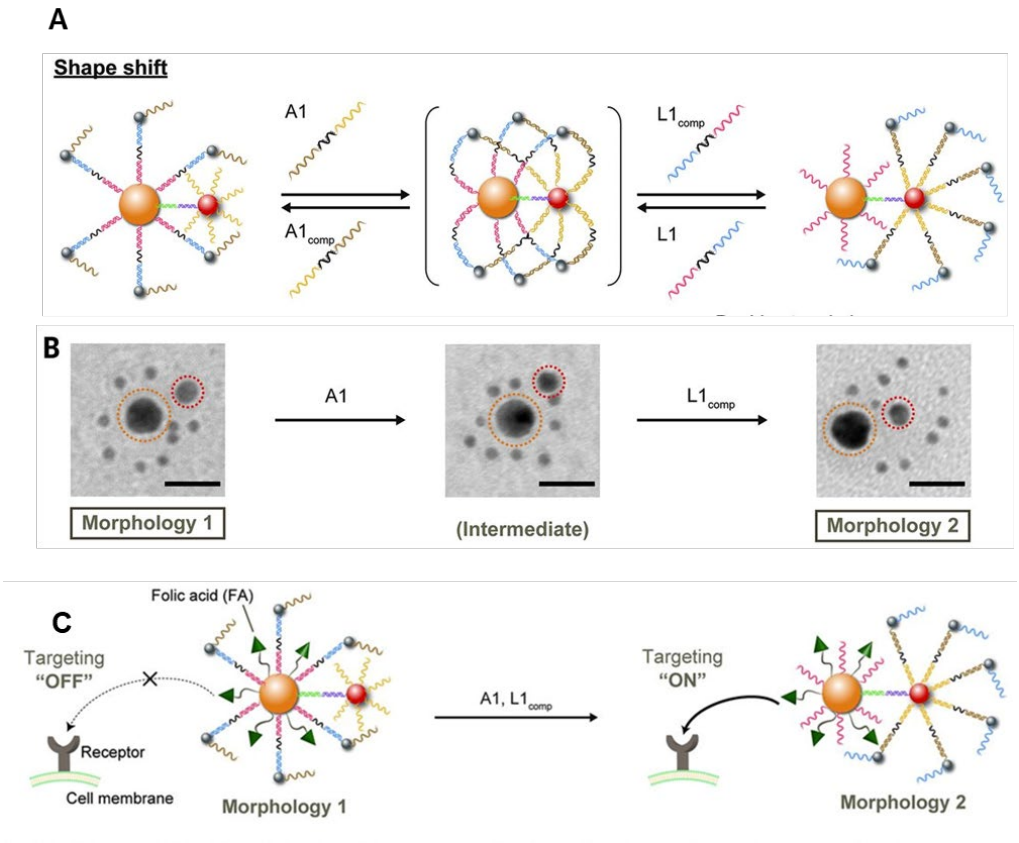

Figure 9. (A) To change the shape of the nanoassembly, attaching strands (A1) were added to anchor small satellites to the medium particle. After that, the detaching strand (L1comp) was added to dislocate L1, resulting in the relocation of small satellites from the large core to the medium satellites (assembly morphology 2). This shape change can be reversed by adding extra attaching and detaching strands, L1 and A1comp. (B) Representative TEM images of the nanoassemblies of morphology 1, intermediate, and morphology 2. They consist of 13-, 6-, and 3-nm gold NPs.The orange and red circles indicate a 13- and 6-nm particle, respectively. Scale bar, 20 nm. (C) In assembly morphology 1, FA is surrounded by satellite NPs, which impedes its targeting property ("OFF" state). Then after the shift to morphology 2, the "hidden" FA is exposed to the outer environment, which activates the cellular uptake property of the assemblies ("ON" state). Reproduced with permission.[98] Copyright 2016, Science.

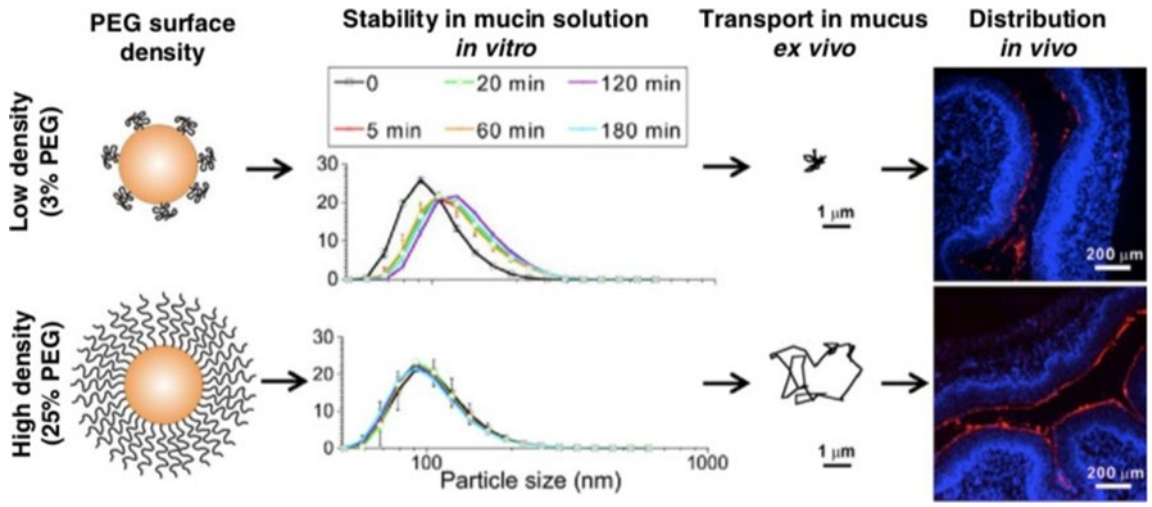

Figure 10. The effects of PEG surface density with mucus in vitro, ex vivo, and in vivo. Above a certain threshold (5% PEG), NPs were more stable in vitro, diffused rapidly ex vivo, and distributed more uniformly in vivo. Reproduced with permission.[101] Copyright 2016, Advanced Drug Delivery Review.

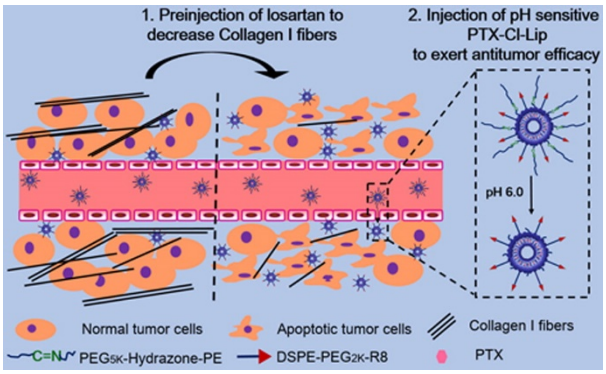

Figure 11. Schematic Illustration about the effect of losartan and the pH sensitive liposomes (PTX-Cl-Lip) in tumor area. Reproduced with permission.[108] Copyright 2015, ACS Applied Materials & Interfaces.

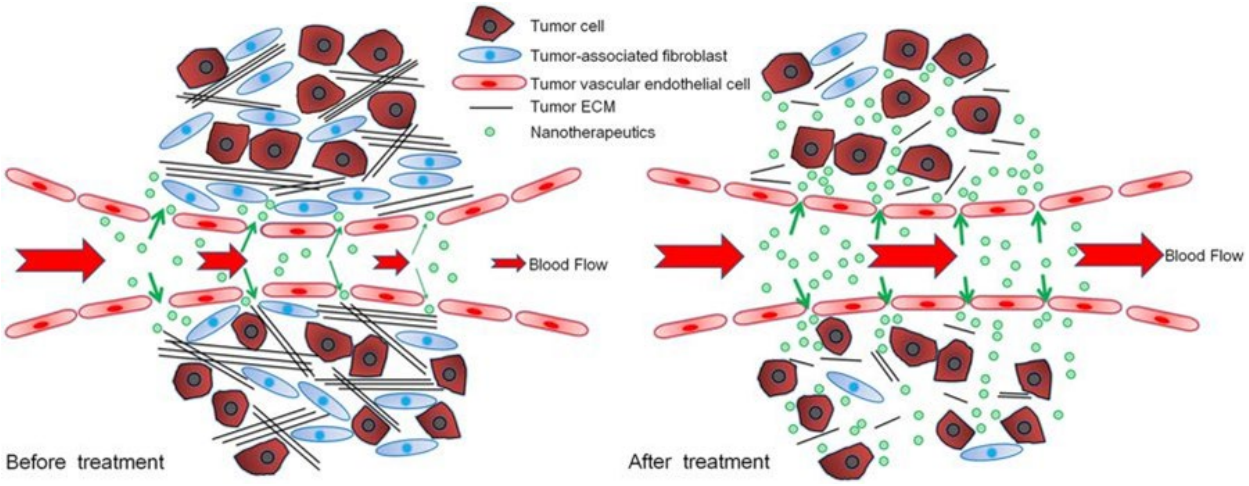

Figure 12. Schematic graphs of the tumor microenvironment and nanotherapeutics delivery to tumors rich in vessels and ECM before and after celecoxib treatment. Before celecoxib treatment, the tumor vessels were leaky and compressed by tumor ECM and TAF, which were a main contributor to the heterogeneous perfusion in tumors and, accordingly, the compromised nanotherapeutics delivery to tumors. As a comparison, celecoxib treatment reduced TAF, disrupted tumor ECM, and repaired tumor vessels to enhance their maturity, which ultimately improved tumor perfusion and enhanced tumor nanotherapeutics delivery. Reproduced with permission.[127] Copyright 2017, Scientific Reports.

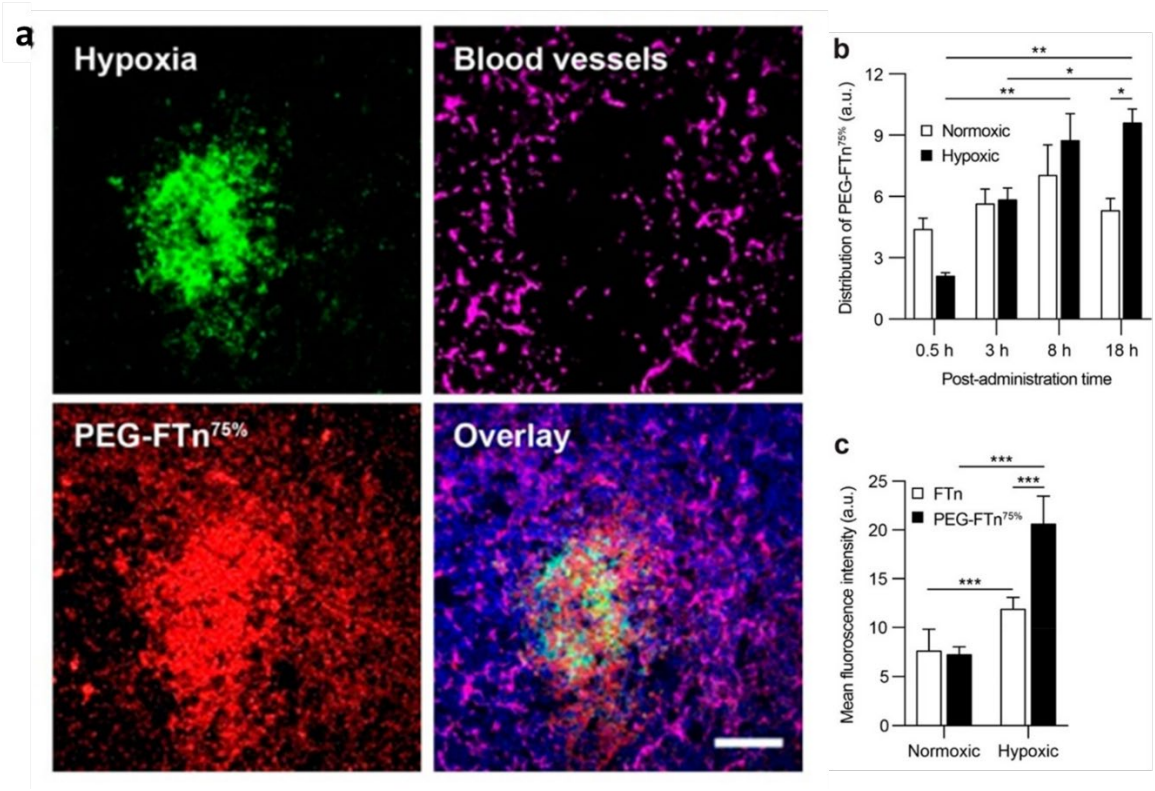

Figure 13. (a) In vivo behaviors of PEG-FTn$^{75\%}$. Representative confocal images showing accumulation of systemically administered PEG-FTn$^{75\%}$ (red) in hypoxic areas (green) within a 3LL-based orthotopic lung tumor tissue. Magenta color represents blood vessels. Scale bar = 100 μm. (b) Image-based quantification of PEG-FTn75% localization in normoxic and hypoxic tumor areas at different time points after the administration (n = 4). (c) Flow cytometry analysis of accumulation of PEG-FTn75%, in comparison to non-PEGylated FTn, in normoxic and hypoxic tumor areas 18 h after the administration. Reproduced with permission.[149] Copyright 2019, ACS Nano.

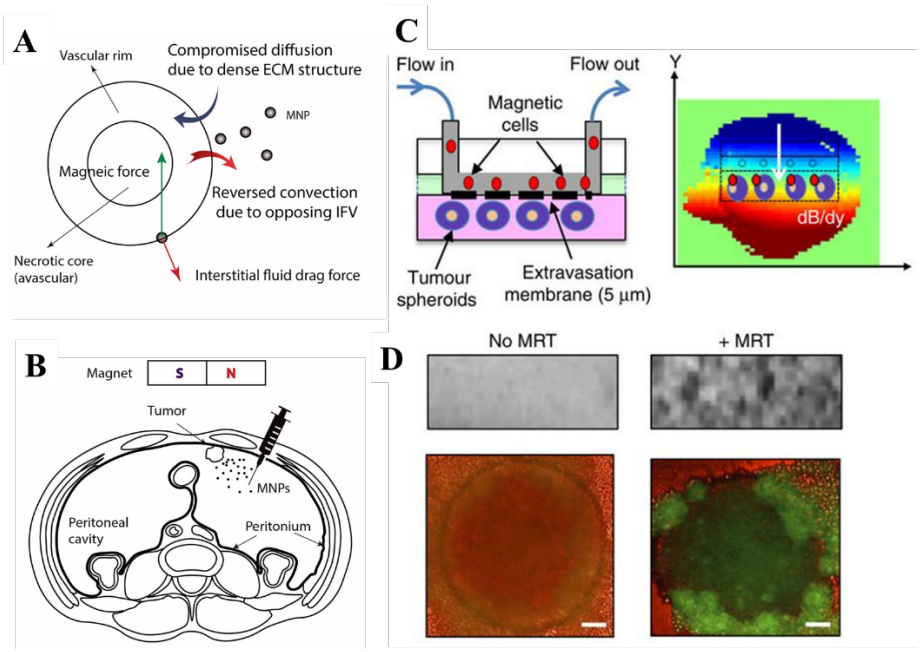

Figure 14. (A) Pathophysiology of tumors gives rise to opposing convective flows of the interstitial fluid at the tumor periphery which repel MNPs. Magnetic forces can be applied to counteract these effects. (B) Schematic of the proposed magnetically assisted Intraperitoneal chemotherapy. Horizontal disposition of the peritoneum targeted with drug-loaded magnetic NPs (MNPs). A permanent external magnet is utilized to impel MNPs across tumor nodules and surpass interstitial barriers. (C) MRT using a novel transendothelial migration (TEM) flow assay. A flow chamber that can accommodate 3D tumor spheroids as well as a vascular endothelial layer. (C, left panel). The TEM flow chamber is placed in the isocenter of an MRI scanner. The resulting heterogeneous magnetic field (dB/dy field) can steer magnetic particles towards the tumor spheroids for increased uptake (C, right panel). (D) Uptake was confirmed by a distortion in the MRI image and a loss of signal compared with when no MRT was applied (D, upper panel). Corresponding fluorescent images of whole spheroids infiltrated with macrophages carrying a reporter adenovirus (Ad-CMV-GFP) are shown in (D, second panel). Scale bar, 100 µm. Reproduced with permission.[157, 159] Copyright 2018, Drug Delivery. Copyright 2015, Nature Communications.

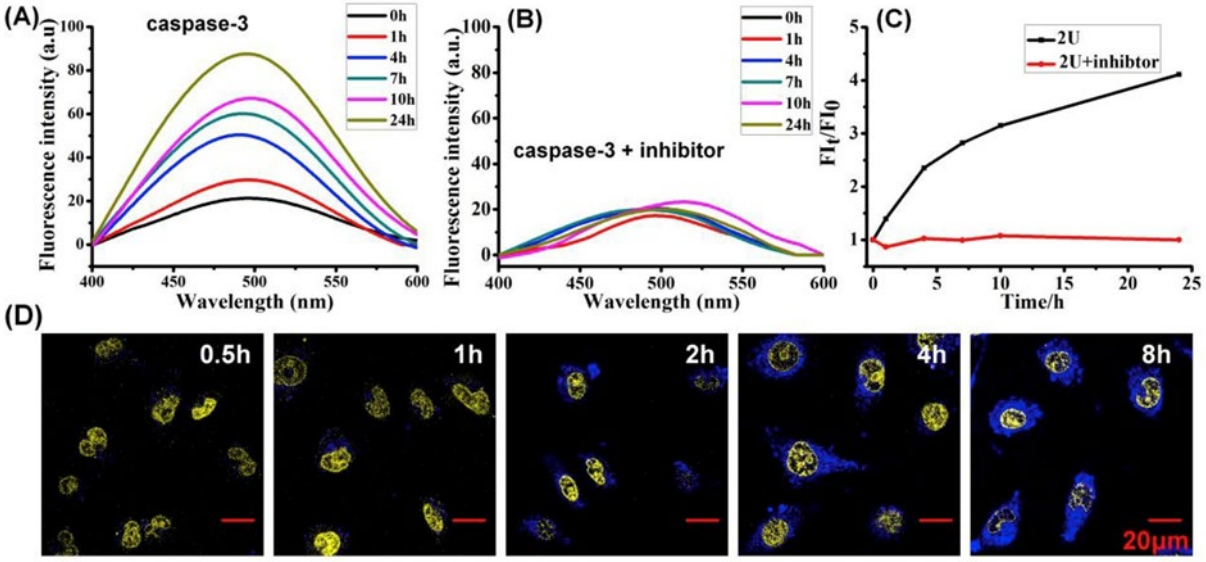

Figure 15. Specific fluorescence 'switch on' performance of STD-NM. Time-dependent fluorescence spectra of TPE in STD-NM after treatment with caspase-3 (A) and caspase-3 with its inhibitor (B). C) The fluorescence intensity ratios of TPE in (A) and (B). FI0: the fluorescence intensity at 0 h, FIt: the fluorescence intensity at different points in time. D) Real-time CLSM images displaying the apoptotic progress of STD-NM stained HUVEC cells at pH 6.5. Nuclei were live stained with DRAQ5 (yellow). All images share the same scale bar (20 μm). Reproduced with permission.[176] Copyright 2019 Biomaterials.

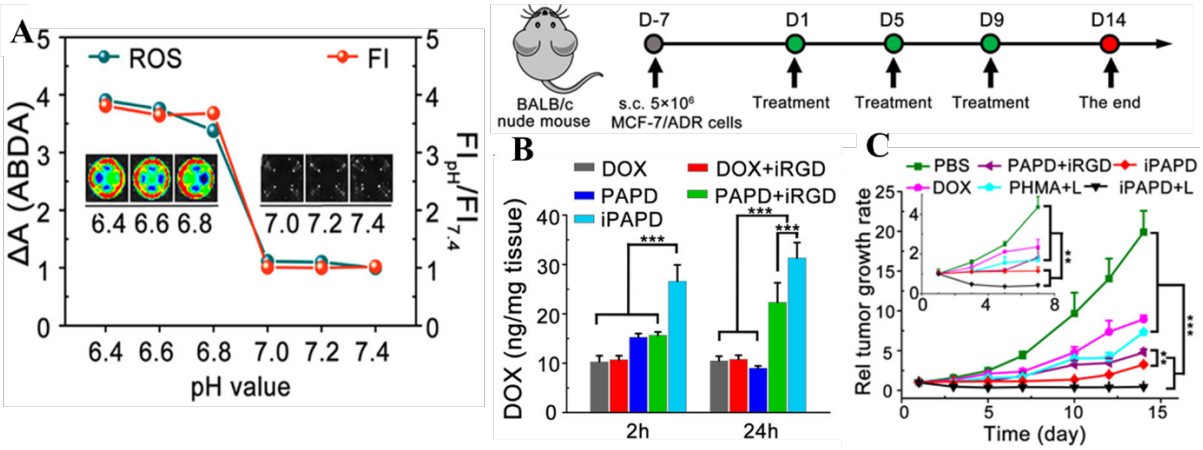

Figure 16. (A) Acid-triggered activation of fluorescence and photodynamic properties of iPAPD NPs (fluorescence imaging was performed at Ex = 640 nm and Em = 680 nm for Ce6). (B) Quantitative examination of DOX distribution in the tumor xenograft 2 or 24 h postinjection (*** $p < 0.01$). (C) In vivo antitumor performance of ATLP NPs. TUNEL staining of the tumor sections. Reproduced with permission.[177] Copyright 2017, American Chemical Society.

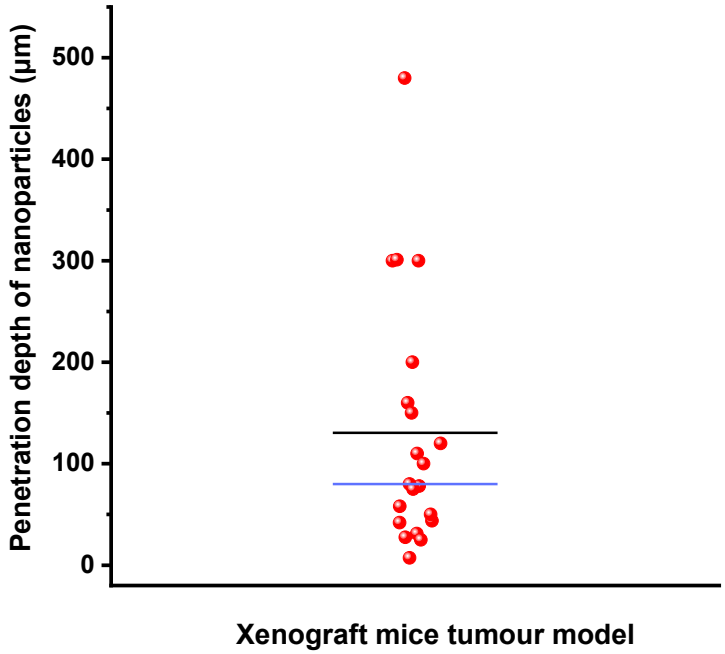

Figure 17. The maximum penetration depth of nanomedicines in xenograft mice tumor models via intravenous injection in 21 publications.[17-18, 61, 63, 132, 135, 146, 185, 194, 198-209] The depth is measured from the tumor vessels. The black and blue line indicates the mean and median, respectively.

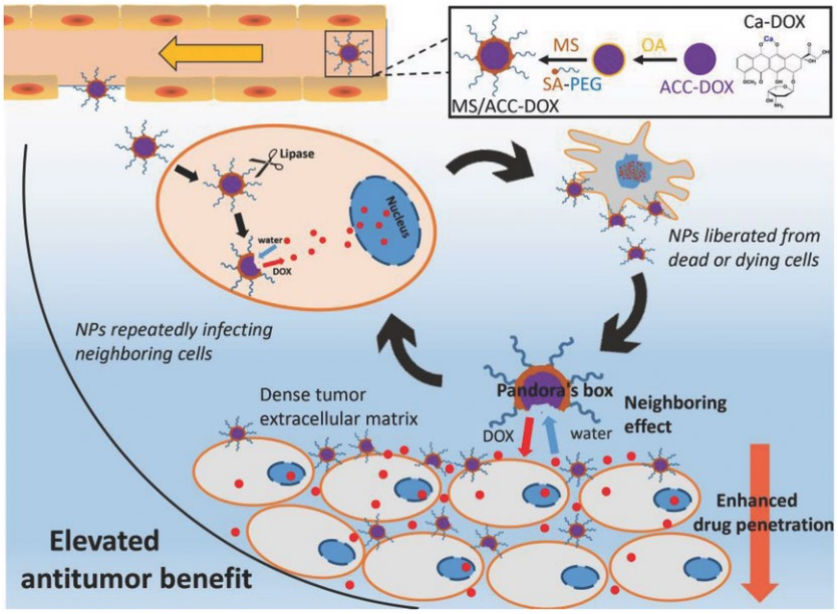

Figure 18. Illustration of formation and elevated antitumor mechanism of "Pandora's box" (MS/ACC–DOX) NPs. Reproduced with permission.[186] Copyright 2018, Advanced Materials.

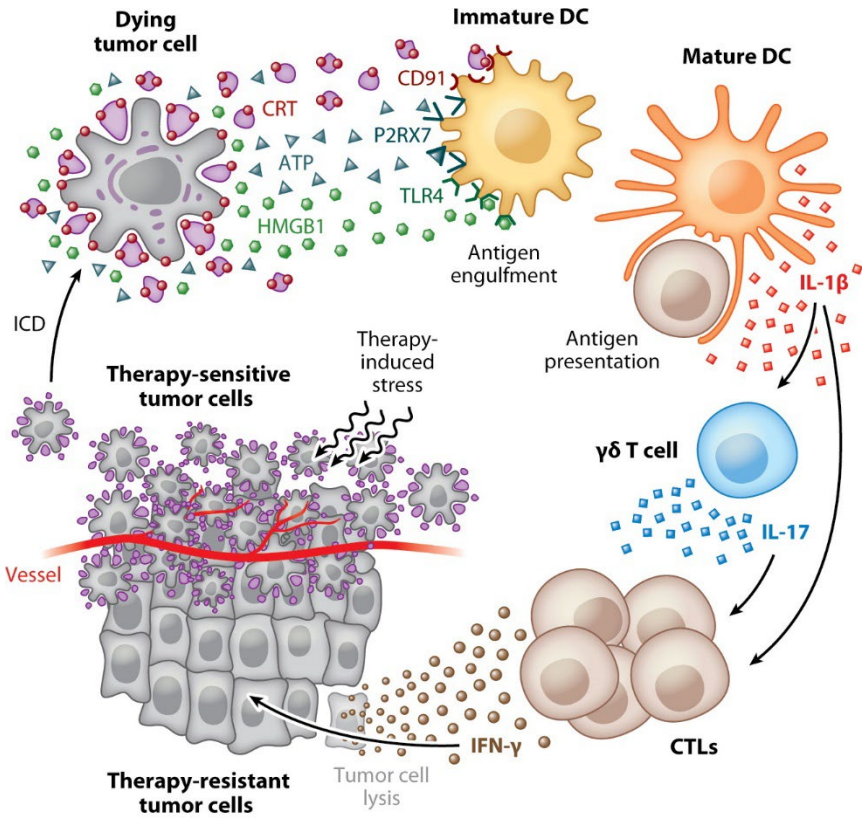

Figure 19. Properties of immunogenic cell death (ICD). As a result of premortem endoplasmic reticulum stress and autophagy, cancer cells responding to ICD inducers expose CRT on the outer leaflet of their plasma membrane at a preapoptotic stage, and secrete ATP during apoptosis. In addition, cells undergoing ICD release the nuclear protein HMGB1 as their membranes become permeabilized during secondary necrosis. CRT, ATP, and HMGB1bind to CD91, P2RX7, and TLR4, respectively. This facilitates the recruitment of DCs into the tumor bed (stimulated by ATP), the engulfment of tumor antigens by DCs (stimulated by CRT), and optimal antigen presentation to T cells (stimulated by HMGB1). Altogether, these processes result in a potent IL-1β- and IL-17-dependent, IFN-γ-mediated immune response involving both γδ T cells and CTLs, which eventually can lead to the eradication of chemotherapy-resistant tumor cells. (Abbreviations: ATP, adenosine triphosphate; CRT, calreticulin; CTL, cytotoxic $CD8^+$ T lymphocyte; DC, dendritic cell; HMGB1, high-mobility group box 1; IFN, interferon; IL, interleukin; TLR, Toll-like receptor. Reproduced with permission.[210] Copyright 2013, Annual Review of Immunology.

Table 1. A summary of recent size/surface charge switch upon pH stimulus.

Nanoplatform	Switchable properties	Triggers	Transition Mechanism	Payload	Ref
PEG-2CHO-Pa-Hyd-DOX	Surface charge switch + Size shrinking	Low pH	1. Detachment of PEG via the cleavage of Schiff base bonds at weakly acidic tumor extracellular pHe. 2. Cleavage of hydrazone bond between Pa and DOX at acidic tumor intracellular pHi.	Doxorubicin	2019[211]
PDEA-b-P(OEGMA-co-PDS)	Size shrinking	Low pH	1. Aggregated micelle-like PDEA blocks were self-disassembled into small linear PDEA blocks at acidic pH.	Paclitaxel	2019[97]
Au@ mPEG-d-PEI /ATRA/siHSP47	Surface charge increase + Size shrinking + hydrophobicity increase	Low pH	1. Detachment of PEG via the cleavage of benzoic imine bond at acidic tumor extracellular pH (pHe). 2. Exposure of hydrophobic chain of ATRA.	HSP47 siRNA	2018[112]
Shell-DMMA-Core	Surface charge switch + Size shrinking	Low pH	1. Cleavage of pH sensitive DMA groups and exposure of positively charged core.	Doxorubicin	2017[63]
DMA-PEI-PDHA	Surface charge switch + Size shrinking	Low pH	1. Cleavage of pH sensitive negative charged DMA. 2. Dissociation of pH sensitive PDHA.	Paclitaxel	2017[212]

Table 2. A summary of recent size/surface charge switch upon overexpressed enzymes.

Nanoplatform	Switchable properties	Triggers	Transition Mechanism	Payload	Ref
DGL/DOX-EGPLGVRGK -PEG-PCL	Size shrinking	MMP-2	Cleavage of MMP-2 sensitive EGPLGVRGK peptide.	Doxorubicin	2018[83]
Ato-ICG-BSA-Gelatin	Size shrinking	MMP-2	Degradation of gelatin.	Atovaquone	2019[140]
PPa–GPLGLAG–PEG	Size shrinking	MMP-2	Cleavage of MMP-2 sensitive GPLGLAG peptide.	Oxaliplatin & doxorubicin	2017[90]
DOX-DGL/ NO-modified HA	Size shrinking	Hyaluronidase	Degradation of hyaluronic acid.	Doxorubicin	2018[213]

Table 3. A summary of recent size/surface charge switch upon hypoxia stimulus.

Nanoplatform	Switchable properties	Triggers	Transition Mechanism	Payload	Ref
Angiopep-2-lipid-poly(MIs)n	Intracellular drug release	hypoxia	Single-electron reduction of hydrophobic P-(MIs)n core to hydrophilic poly-aminoimidazoles by intracellular nitroreductases.	Doxorubicin	2018[72]
DOX/CP-NI NPs	Surface charge increase + intracellular drug release	hypoxia	Bioreduction of hydrophobic 2-nitroimidazole to hydrophilic 2-aminoimidazoles.	Doxorubicin	2016[147]
DOX/NI-CD mesoporous silica NPs				Doxorubicin	2018[214]
DOX/ CM-Dox-NI NPs				Doxorubicin	2014[80]
PAP-FC NPs	Increased positive surface charge	hypoxia	Cleavage of hypoxia-responsive azobenzene.	Doxorubicin	2018[215]

Table 4. A summary of recent size/surface charge switch upon multi-stimuli.

Nanoplatform	Switchable properties	Multi-stimuli types	Functionalized component	Tumor model	Ref
RGD-PEI-SS-PLA/PTX@MMP-2 cleavage peptide nanoclusters	Size shrinking + intracellular drug release	MMP-2 + Redox	MMP-2 cleavage peptide + disulfide bond	MCF-7 human breast cancer	2019[86]
DGL/DOX-EGPLGVRGK -PEG-PCL	Size shrinking + intracellular drug release	MMP-2 + pH	EGPLGVRGK peptide + pH sensitive hydrazone bond	4T1 murine breast tumor xenograft	2018[83]
PEG113-P(API-PTX)20 BCPs	Surface charge switch + size shrinking	Low pH + Redox	Protonation of pH sensitive imidazole groups + disulfide bond	4T1 breast tumor + BxPC3 human pancreatic adenocarcinoma tumor	2018[216]
Mesoporous silica-coated gold NPs	Size shrinking + surface charge switch	pH + NIR + Redox	PEG-tailed thermosensitive polymers + RGD-tailed poly(disulfide)s + pY^{-}/Gu^{+} motifs	MCF-7 tumor xenograft	2017[217]
Polypeptide-doxorubicin NPs	Size shrinking + intracellular drug release	Ultrasound + pH	LHRH + ELP + C8 peptides + hydrazone bond		2017[218]

Table 5. A summary of recent NPs for deep tumor penetration by optimizing surface biochemistry.

Nanoplatform	Surface substances for deep penetration		Ref
Porous silicon	Sndecylenic acid		2016[219]
21-arm star block nanoscale copolymers	Zwitterionic poly(carboxybetaine) (PCB)		2016[220]
DOX-DGL/HN/iRGD	iRGD		2018[221]
iRGD peptide amphiphile-HB			2018[222]
iNGR-liposome/DOX	Tumor-penetrating peptide	iNGR (CRNGRGPDC)	2017[223]
PEG/ Iron-oxide NPs		LyP-1 (CGNKRTRGC)	2017[107]
PEG crosslink micelles	cRGD + cell-penetrating peptides (TAT peptide)		2017[224]

Table 6. A summary of recent methods for the modulation of ECM via external physical energy.

Physical energy	Mechanism	Ref
Very low intensity ultrasound	Insonation	2019[225]
NIR light	Photothermal ablation	2019[226]
Alternating magnetic force	Magnetic NPs-based hyperthermia	2017,[227] 2018[228]

Table 7. A summary of recent multi-strategies combined NPs for tumoral deep penetration.

Nanoplatform	Functionalized component	Combined strategies	Therapeutics	Tumor model	Ref
PCB-tBu-DOX	Zwitterionic PCB + pH-sensitive acylhydrazone bonds	Surface chemistry facilitated + drug release	Doxorubicin	H22 tumor	2016[220]
RGD-PEI-SS-PLA/PTX@MMP-2 cleavage peptide nanoclusters	RGD-$\alpha_v\beta_3$ integrin + MMP-2 cleavage peptide + disulfide bond	Surface chemistry facilitated + Size shrinking + intracellular drug release	Paclitaxel	MCF-7 human breast cancer	2019[86]
AQ4N-Cu(II)-(DOX)2-Cu(II)-metal–organic NPs	Acidic cleaved host–metal coordination bonds + a photosensitizer (ZnPC)	Size shrinking + Hypoxic normalization ($^1O_2$ generation) + intracellular drug release	Doxorubicin & bioreducible banoxantrone (AQ4N)	HepG2 hepatocellular carcinoma spheroids	2018[79]
DOX/CP-NI NPs	NIR light-activated dithiophene-benzotriazole moiety+ 2-nitroimidazole	Hypoxic normalization ($^1O_2$ generation) + intracellular drug release	Doxorubicin	HeLa tumor	2016[147]
SPIO/PTX-NP / PCL-PEG-RGD	Superparamagnetic iron oxides + RGD-$\alpha_v\beta_3$ integrin	Magnetic directing + surface chemistry facilitated	Paclitaxel	CT26 tumor	2014[229]
Mag-pH-DS	Iron oxide NPs + folate-PAMAM dendrimers + pH responsive liposomes	Magnetic directing + size shrinking + surface chemistry facilitated	-	Hela cells tumor spheroids	2016[230]
Platinum-PEG nanowarms	Hyaluronic acid shells + NIR laser sensitive nitric oxide donor + indocyanine green	Size shrinking + intracellular drug release + modulation of tumor microenvironment	Doxorubicin	4T1 breast cancer xenograft	2018[231]
DOX-DGL/HN/iRGD	iRGD + hyaluronic acid shells + indocyanine green + nitric oxide donors	Surface chemistry facilitated + size shrinking + modulation of tumor microenvironment (hyperthermia & NO release)	Doxorubicin	4T1 breast cancer xenograft	2018[221]

Table 8. A summary of recent deep penetrated NPs with theranostic function.

Nanoplatform	Component for deep penetration	Component for imaging	Imaging tool	Ref
PLGA NPs	RGD-$\alpha_v\beta_3$ integrin + superparamagnetic iron oxides	Superparamagnetic iron oxides	MRI	2014[229]
H-MnO2-PEG/C&D nanoshell	Hollow mesoporous MnO_2 shell (break-up under acidic pH)	MnO_2 + Ce6	T1-weighted MRI + fluorescence	2017[232]
Platinum (Pt)-PEG nanowarms	Pt + PEG	Pt	Photoacoustic imaging + CT	2018[231]
DOX/CP-NI NPs	Dithiophene-benzotriazole moiety+ 2-nitroimidazole	Dithiophene-benzotriazole moiety	NIR imaging	2016[147]
IR780 nanodroplets	Perfluoropentane (induced vascular disruption under ultrasound)	IR780	Fluorescence + ultrasound + photoacoustic imaging	2019[233]

Deep penetration of nanoparticles in the tumor environment is vital in producing successful nanomedicines. This review emphasizes the need of smart nanotechnology to facilitate the deep penetration of nanomedicines in tumors.

Smart nanotechnologies to target tumor with deep penetration depth for efficient cancer treatment and imaging

*Xue Feng, Hannah Dixon, Harriet Glen-Ravenhill, Sena Karaosmanoglu, Quan Li, Li Yan, Xianfeng Chen**

Keywords: Nanoparticles; deep penetration; tumor; tumor microenvironment; cancer

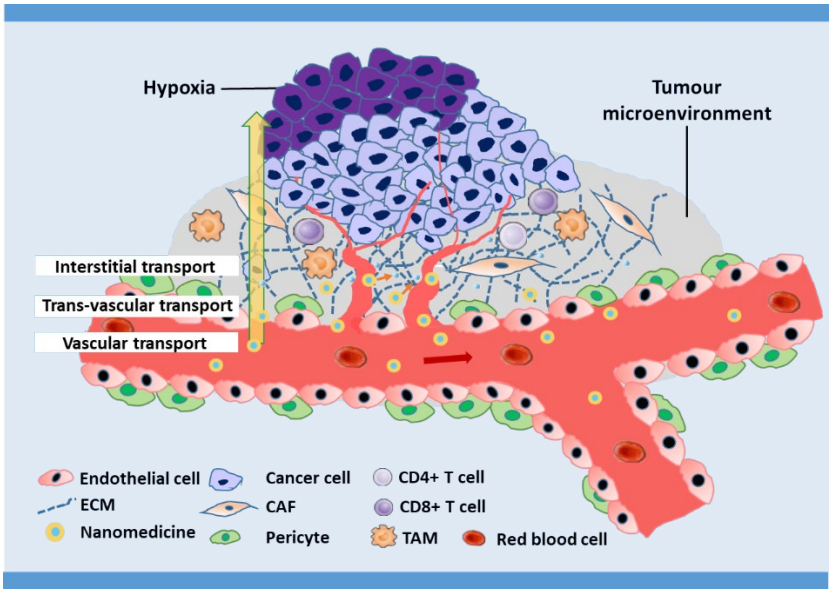

Biography:

Xue Feng is currently a Ph.D. student in the Institute for Bioengineering, School of Engineering at the University of Edinburgh, under the supervision of Dr Xianfeng Chen. She received her MSc degree from the University of Manchester in 2017. At present, her research interests are focused on biomaterials, magnetic nanomaterials, and the development of their application in anticancer therapy.

Li Yan obtained his Doctorate of Philosophy in 2015 from City University of Hong Kong, under the supervision of Dr. Xianfeng Chen and Prof. Wenjun Zhang. He is currently a research fellow at the Faculty of Pharmacy and Pharmaceutical Sciences at Monash University in Australia. His research interest includes nanomedicine for drug delivery, microneedle technology for transdermal delivery and biosensing.

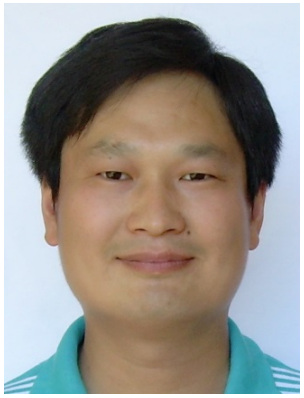

Xianfeng Chen received his Doctor of Philosophy (DPhil) in Materials Science from the University of Oxford. He is currently a Lecturer in Chemical Engineering, working in the Institute for Bioengineering, School of Engineering at The University of Edinburgh. He holds a visiting professorship at Guangzhou Medical University, China. His research is focused on biomaterials, biomedical engineering, and the application of materials in biology and medicine with a focus in anticancer therapy.